A viscoelastic and afterslip postseismic deformation model for the 1964 Alaska earthquake

Hisashi Suito[1] and Jeffrey T. Freymueller[2]

Received 25 July 2008; revised 13 July 2009; accepted 27 July 2009; published 11 November 2009.

[1] We developed a 3-D viscoelastic model, in concert with an afterslip model, to describe the postseismic deformation following the 1964 Alaska earthquake. Our model incorporates a realistic geometry including an elastic slab with very low dip angle. These geometric factors are important and require a reanalysis of the 1964 coseismic model. Our coseismic model differs from previous models in that the Montague Island splay fault extends farther along the Kenai Peninsula coast, and as a result, slip on the megathrust in that region is smaller. We computed postseismic deformation models using a range of mantle viscosities with Maxwell relaxation time τ of 1 to 50 years, with a best estimate of 20 years. The viscoelastic model explains most of the trenchward motion observed in the present velocity field but has little impact on cumulative 1965 to present uplifts. After removing the viscoelastic response, the largest residual cumulative uplifts were located downdip from areas of largest coseismic slip area, and we explain them using an afterslip model, constrained in space by the observed cumulative postseismic uplifts and in time by tide gauge records. No single mechanism can explain both the 30 years of cumulative uplift and the present velocities, but a combination of viscoelastic relaxation, afterslip, interseismic elastic deformation, and motion of southern Alaska relative to North America explains the first-order features of the observations. Forty years after the earthquake, the present-day velocities contain a significant component of postseismic deformation, so very long lived postseismic deformation plays an important role in the subduction zone earthquake cycle for great earthquakes.

Citation: Suito, H., and J. T. Freymueller (2009), A viscoelastic and afterslip postseismic deformation model for the 1964 Alaska earthquake, *J. Geophys. Res.*, *114*, B11404, doi:10.1029/2008JB005954.

1. Introduction

[2] The M_w = 9.2 1964 Alaska earthquake was the second largest instrumentally recorded earthquake, and it triggered long-lived postseismic deformation continuing more than four decades after the event [e.g., *Cohen and Freymueller*, 2004, and references therein]. The slow surface motions that accompany postseismic stress redistribution and interseismic stress accumulation can provide new insights into the rheology and mechanics of the lithosphere and asthenosphere. However, limitations in the temporal and spatial distribution of data, and the sheer size of the area affected, have made the development of a comprehensive model of postseismic deformation difficult. Past models of the postseismic deformation in the Cook Inlet region focused on afterslip because viscoelastic-only models did a poor job at predicting the cumulative uplift observations [*Cohen and Freymueller*, 1997; *Zweck et al.*, 2002b]. More recently, *Sauber et al.* [2006] used 3-D elastic dislocation models and 2-D finite element models to study postseismic and interseismic deformation for Kodiak Island, and showed that both afterslip and viscoelastic relaxation contributed significantly to postseismic deformation there. In the present paper, we constructed a three-dimensional viscoelastic finite element model for the region surrounding the entire 1964 earthquake rupture area, with realistic plate and crustal structures based on the seismic velocity structure and the spatial distribution of the microearthquakes. We show that a combination of viscoelastic relaxation and afterslip is required to explain the observed postseismic deformation, and determine a best model for the present horizontal velocities based on postseismic deformation and an interplate slip deficit distribution. We determined the relative importance of each mechanism for each of the available data sets.

[3] The 1964 Alaska earthquake rupture extended 600–800 km from Prince William Sound (PWS) along the entire Kenai Peninsula to Kodiak Island along a 200–250 km wide zone (Figure 1), with average fault slip of more than 10 m [*Kanamori*, 1970]. The rupture distribution of the 1964 earthquake was highly nonuniform, with most of the moment resulting from the rupture of two separate asperities [*Christensen and Beck*, 1994]. The largest asperity lies offshore and beneath PWS and the eastern Kenai Peninsula, with >20 m slip. A smaller asperity beneath Kodiak Island also ruptured with ~15 m slip, but less slip occurred in the

[1]Geography and Crustal Dynamics Research Center, Geographical Survey Institute, Tsukuba, Japan.
[2]Geophysical Institute, University of Alaska Fairbanks, Fairbanks, Alaska, USA.

0148-0227/09/2008JB005954$09.00

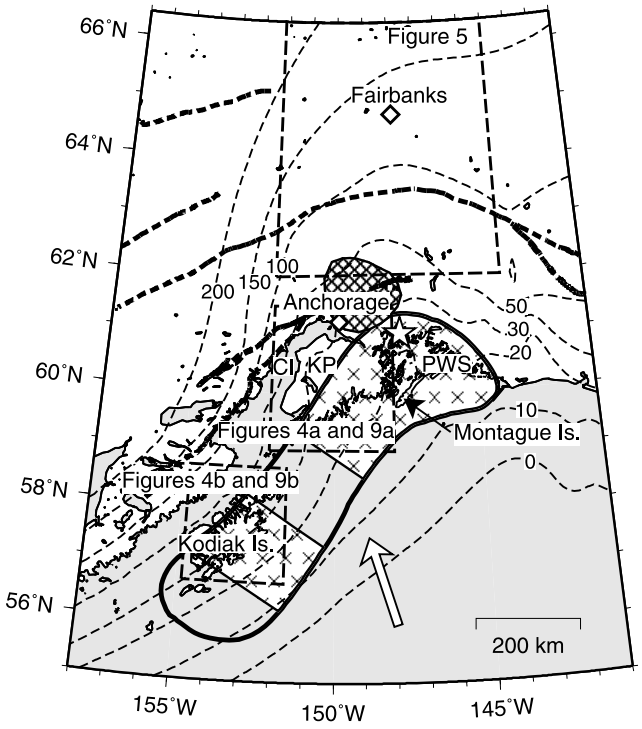

Figure 1. Location map of southern Alaska. The white star and thick line indicate epicenter and source area of the 1964 Alaska earthquake, respectively. The areas shaded with crosses denote the asperities of Prince William Sound (PWS) and Kodiak. The dark shaded area denotes the area of slow slip event (SSE) reported by *Ohta et al.* [2006]. Thin and thick dashed lines indicate the isodepth contour of subducting Pacific plate and the traces of inland faults, respectively. The white arrow shows the Pacific–North America relative motion direction. Outlined areas of Figures 4, 5, and 9 are also shown by dashed lines. CI, Cook Inlet; KP, Kenai Peninsula; PWS, Prince William Sound.

area between these two asperities [*Christensen and Beck*, 1994; *Holdahl and Sauber*, 1994; *Johnson et al.*, 1996; *Santini et al.*, 2003]. *Cohen and Freymueller* [2004] included an extensive critical summary of past coseismic models. Although the models differ in detail, all have common elements, including large slip in the two main asperities, and a region of low slip between them. In this study, we adjust the coseismic model based on an improved model geometry, and reassess the horizontal and vertical coseismic data to identify the observations that best constrain aspects of the coseismic model. We also make use of information from the recently published model of *Ichinose et al.* [2007], which reassessed the seismic data.

[4] Many researchers have reported the postseismic deformation following the 1964 earthquake as inferred from leveling studies [*Brown et al.*, 1977; *Cohen et al.*, 1995], tide gauge analyses [*Brown et al.*, 1977; *Savage and Plafker*, 1991; *Gilpin et al.*, 1994; *Gilpin*, 1995; *Cohen and Freymueller*, 1997; *Larsen et al.*, 2003], GPS observations [*Savage et al.*, 1998; *Freymueller et al.*, 2000] and through comparisons of recent GPS height determinations with earlier leveling observations [*Cohen et al.*, 1995; *Cohen and Freymueller*, 1997]. *Zweck et al.* [2002a, 2002b] modeled the present-day and cumulative postseismic deformation following the 1964 earthquake using an afterslip model. They ignored the viscoelastic response to the earthquake because the predictions of previous viscoelastic modeling studies [e.g., Piersanti et al.,1997] predicted the wrong sign for the cumulative postseismic uplift data, while afterslip provided a ready explanation for those same observations [*Cohen et al.*, 1995; *Cohen and Freymueller*, 1997]. Although afterslip models are able to explain the present GPS velocities from southern Alaska, they require afterslip extending to great depths, which may not be realistic. In addition, postseismic deformation appears to extend several hundred km inland from the trench, which is impossible to explain with an afterslip model. Improved data sets for cumulative postseismic vertical displacements, present surface velocities, and tide gauge records [*Larsen et al.*, 2003] are now available, and we use these new data to constrain our postseismic model. *Sauber et al.* [2006] reported that multiple mechanisms are needed to explain the crustal deformation across Kodiak Island, so a reassessment of postseismic deformation in the Cook Inlet and the development of a complete 3-D model are now appropriate.

[5] In order to complement previous modeling efforts and understand the postseismic deformation following the 1964 Alaska earthquake, we have implemented a 3-D viscoelastic model, in concert with afterslip models, using the Finite Element Method. Of particular importance is the inclusion of a dipping elastic slab, which has a dramatic impact on the viscous mantle flow and the model postseismic deformation. *Hu et al.* [2004] used similar model geometry in their 3-D finite element model for the 1960 Chile earthquake. Using the viscoelastic model, we show that measurements of postseismic uplift on Kodiak Island and the Kenai Peninsula are largely insensitive to viscoelastic effects, allowing us to use these data to constrain the afterslip distribution and time history. In contrast, the postseismic contribution to the present horizontal surface velocities is largely due to viscoelastic relaxation. This allows us to use far-field postseismic displacements to constrain this component of the postseismic deformation. This convenient separation of effects results from the combined effect of subduction geometry and time, and we exploit it to present a combined postseismic deformation model. Near-field present velocities are dominated by the elastic deformation from the shallow interseismic slip deficit distribution, and tradeoffs between the postseismic model and present slip deficit distribution are significant.

2. Available Data

[6] The postseismic deformation depends on the coseismic slip distribution. This section describes the coseismic and postseismic data we use to constrain the models. We use only surface geodetic data here. Seismic records from the earthquake were sufficient to identify the two main regions of high slip, and determine their locations subject to assumptions about the rupture velocity [*Christensen and Beck*, 1994]. *Nettles et al.* [2005] recently reanalyzed the surface wave data over multiple orbits to estimate the earthquake magnitude as M_w 9.3. *Ichinose et al.* [2007] recently reanalyzed of the seismic data, in combination with

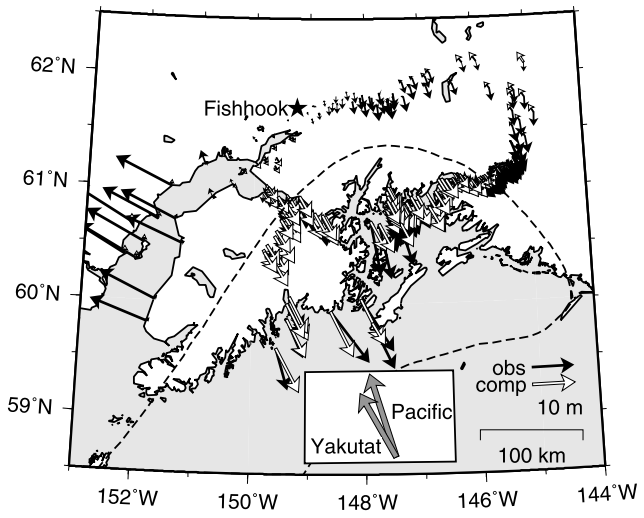

Figure 2. Computed coseismic horizontal displacements (white vectors) relative to the Fishhook (black star), as compared with the observations compiled by *Snay et al.* [1987] (black vectors). Inset shows the Pacific–North America and Yakutat–North America relative motion direction. The large vectors pointing WNW in the western part of the Kenai peninsula are considered to be poorly determined (see also Text S1).

tsunami and geodetic data, and produced an updated slip model. Although tsunami waveform data provides important constraints on slip at shallow depths on the megathrust [*Johnson et al.*, 1996], we did not directly incorporate these data in our model, but we based our model on the slip distribution determined by *Johnson et al.* [1996] using these data.

2.1. Coseismic Displacements

[7] We used horizontal displacements computed from triangulation data by the National Geodetic Survey [*Parkin*, 1972; *Snay et al.*, 1987], and used vertical displacements from repeated precise leveling [*Plafker*, 1972] and from measurements of tide level change made soon after the earthquake [*Small and Wharton*, 1972]. Below we describe the observations, discuss the biases in these data, and identify the critical observations that we used in adjusting the coseismic model.

2.1.1. Horizontal Coseismic Displacements

[8] Two solutions for the horizontal displacements [*Parkin*, 1972; *Snay et al.*, 1987] are available. Differences between the two solutions were discussed in the appendix of *Holdahl and Sauber* [1994] and the auxiliary material (Text S1 and Figure S1).[1] We take a slightly different approach to using the horizontal data compared to *Holdahl and Sauber* [1994] (and *Johnson et al.* [1996]). (see detail in Text S1). We think the systematic biases in these data preclude their use in an inversion model, and instead require our forward model to match specific important first-order features of the data. We used the magnitude of the horizontal displacements as a general constraint, although we gave more weight to the magnitude of the vertical observations, which do not suffer from possible scale biases.

[9] The first important constraint from the horizontal data is that displacements on the western Kenai Peninsula are much smaller than those in the eastern Kenai Peninsula (Figures 2 and S1). This is most clear in Parkin's solution, although both solutions show a westward decrease in displacement (compare Prince William Sound to the eastern Kenai Peninsula). A similar pattern is seen in the present horizontal velocities [*Freymueller et al.*, 2008]. We interpret this as evidence for lower average slip on the megathrust in the western Kenai segment or a shallower downdip limit of slip, indicating a profound change in slip along strike. The small northward directed displacements in Parkin's solution are due mainly to the use of Fishhook as the reference point.

[10] The second important constraint is the change of the orientation of the vectors, which result in a fan-like pattern of displacements. As noted by *Cohen and Freymueller* [2004], this change in azimuth is matched by a similar change in the present velocities from GPS [*Freymueller et al.*, 2008]. Displacements on the eastern Kenai Peninsula are directed opposite to the Pacific–North America plate convergence direction, while displacements in eastern Prince William Sound are directed opposite to the Yakutat–North America convergence direction estimated by *Fletcher and Freymueller* [2003]. We interpret these data as requiring a lateral change of rake angle on the slip plane, from the Pacific–North America direction in the west to the Yakutat–North America direction in the east. *Ichinose et al.* [2007] did not use the horizontal data, but their inversion model estimates a similar rake variation. *Holdahl and Sauber* [1994] allowed for variation in rake in their solution.

2.1.2. Vertical Coseismic Displacements

[11] Vertical coseismic displacements come from two sources. Precise leveling surveys were repeated after the earthquake across much of Alaska to measure displacements and reestablish survey control. These data provide vertical displacements accurate to a few cm or better [*Plafker*, 1972]. Preearthquake leveling benchmarks near the coastal areas were very sparse, although far-field data are abundant. As a result, the leveling data are highly precise but poorly distributed. A more useful data set comes from measurements of coseismic tide level change (Figure 3), made primarily by a USGS team in the months after the earthquake [*Plafker*, 1972]. These show subsidence in most of the region, except for Prince William Sound where large uplifts were observed.

[12] Use of the coseismic tide level changes is not without pitfalls. The tidal range in the region is generally several meters, and different marine plants and animals have varying abilities to survive aerial exposure. Care was taken in the field to account for this, but these measurements have an intrinsic uncertainty much greater than instrumental observations [*Small and Wharton*, 1972]. We show in Figure 3 and use the measurements for which Plafker assigned the greatest confidence, and where measurements were dense we adopted representative measurements rather than including all data. Not shown in Figure 3 for reasons of scale are the ~10 m uplift measurements from the southwest end of Montague Island, location showed by a circle in Figure 3. These extreme uplifts were caused by slip on high-

[1] Auxiliary materials are available in the HTML. doi:10.1029/2008JB005954.

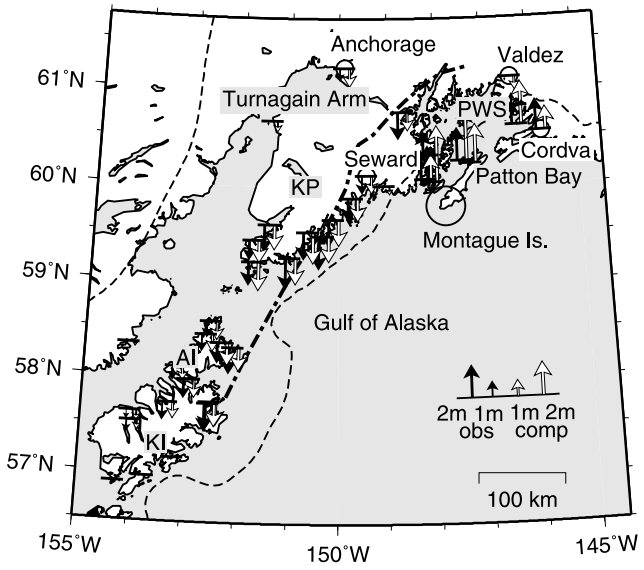

Figure 3. Computed coseismic vertical displacements (white), as compared with the observations (black) compiled by *Plafker* [1972]. The dashed and dot-dashed lines indicate the zero line and the approximate axis of maximum coseismic subsidence from *Plafker* [1972], respectively. Circle shows the SW corner of Montague Island. At this location, splay faulting produced localized 10 m uplifts. Only representative vertical displacements are shown in PWS for clarity. AI, Afognak Islands; KI, Kodiak Islands; KP, Kenai Peninsula; PWS, Prince William Sound.

angle splay faults that broke the surface on either side of the island. The throw estimates on the fault (10 m) are quite precise, based on the surface offsets.

2.2. Postseismic Observations

[13] There is now a rich set of postseismic observations for the 1964 Alaska earthquake, described in detail by *Cohen and Freymueller* [2004]. However, the time history of displacements is not uniform. Precise leveling was repeated along one line near Anchorage for a decade after the earthquake, but no measurements were made from the mid-1970s until the early 1990s when GPS observations began, except for the sparse permanent tide gauges. In this paper we constrain postseismic deformation models using observations that cover three distinct time periods: cumulative vertical displacements over a ~30 year period (1965 to 1990s), continuous tide gauge records (1964 to 2001), and current GPS horizontal velocities (1993–2007).

2.2.1. Cumulative Vertical Displacements

[14] Cumulative vertical displacements mainly come from measurements of elevation change between the 1960s and 1990s (Figure 4). The 1960s measurements on the Kenai Peninsula come from precise leveling surveys in 1964–1965 [*Plafker*, 1972], while the 1990s measurements were made using GPS [*Cohen and Freymueller*, 1997, 2004]. Uncertainties in these data are dominated by errors in the geoid model needed to convert between geometric and orthometric heights, and relative geoid height errors are 10–20 cm across the network due to poor gravity control [*Cohen and Freymueller*, 1997, 2004]. The published displacements for this region are uplift relative to Seward. Vertical displacements from the Kodiak Island region come from repeated tidal benchmark surveys 29 years apart [*Gilpin et al.*, 1994; *Gilpin*, 1995]. Because the same kinds

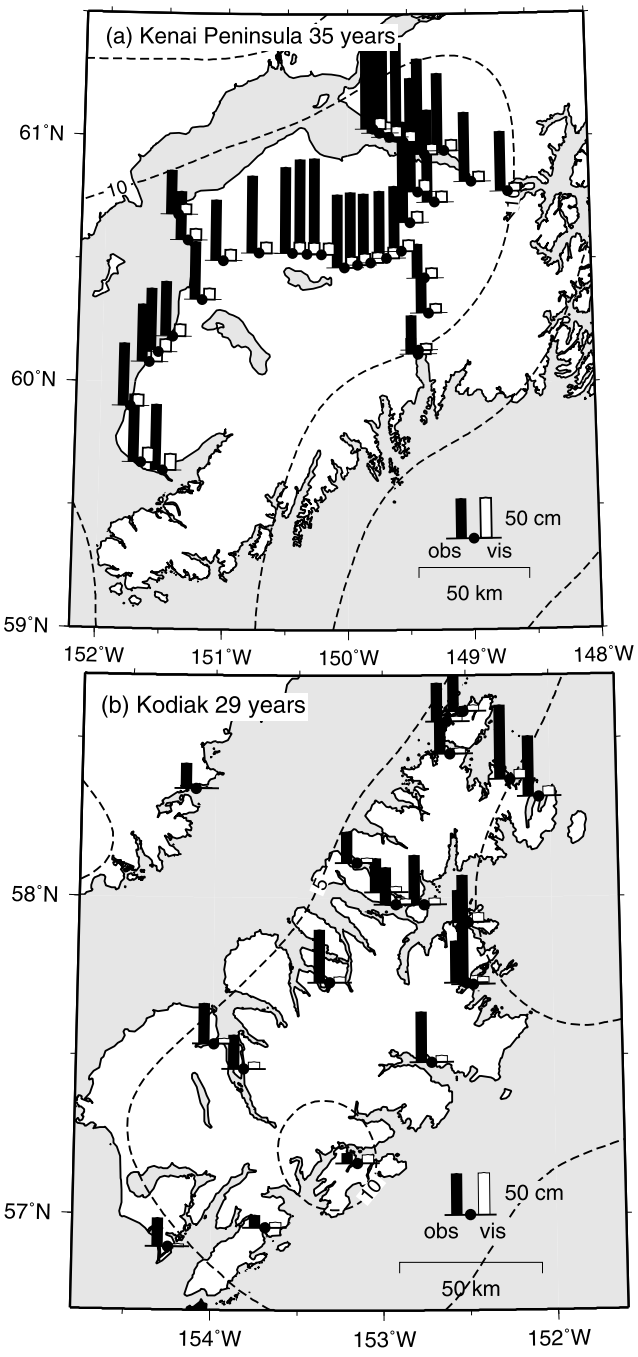

Figure 4. Computed postseismic uplift caused by viscoelastic response. (a) Time span for 35 years in Kenai Peninsula, as compared with the observation (black bar) by combination of leveling surveys and GPS surveys, and tide gauge data at leveling benchmark [*Cohen and Freymueller*, 2004]. (b) Time span for 29 years in Kodiak Island, as compared with the observation (black bar) by repeated tidal benchmark surveys at tidal benchmark data [*Gilpin et al.*, 1994; *Gilpin*, 1995]. (See also Figure S4a for across the entire region.)

of measurements were made in both surveys, significant systematic errors are unlikely, and measurement precision is ~10–20 cm.

[15] The cumulative vertical displacements are dominated by postseismic deformation, but also include uplift due to interseismic elastic strain from the slip deficit in the shallow seismogenic zone. The Kenai measurements also include a contribution from uplift due to glacial isostatic adjustment to recent ice melting. We converted the vertical displacements relative to Seward to absolute vertical displacements by adding the observed total 1965–2000 uplift of the Seward tide gauge, +21 cm [*Larsen et al.*, 2003]. We removed the total 29-year (Kodiak) or 35-year (Kenai) vertical motion due to the melting of ice based on a GIA model [*Larsen et al.*, 2005; C. F. Larsen, personal communication to J. T. Freymueller, 2009]. The ice correction is negligible for the Kodiak Island sites, but ranges from 10 to 25 cm uplift for the Kenai sites. Finally, we removed the vertical motion caused by the elastic response to the slip deficit in the shallow seismogenic zone. We used an earlier iteration of the interseismic elastic model discussed later in this paper for that purpose. For the remainder of this paper, we refer only to the final corrected uplift data, which we assume represent purely postseismic uplift.

[16] Cumulative postseismic uplift is ~50–100 cm both in the Kodiak region (Figure 4b) and Kenai Peninsula (Figure 4a). The largest uplift in the Kodiak region is 108 cm, measured by the permanent tide gauge. On the Kenai Peninsula, cumulative uplift on the western part of the peninsula is typically ~50 cm, with much larger uplift measured in the central and eastern part of the peninsula. The largest uplifts reach 80–90 cm along Turnagain Arm south of Anchorage. The time history of this uplift is poorly constrained, except at the tide gauges. Repeated leveling of a line along Turnagain Arm, extending trenchward from Anchorage, showed relative vertical motion of 20 cm between sites along the line within the first year after the earthquake, and repeated leveling is consistent with roughly half of the postseismic uplift occurring within the first several years after the earthquake [*Brown et al.*, 1977].

[17] *Zweck et al.* [2002b] reported and used measurements of cumulative horizontal displacement. These estimates came from comparing angles between triangulation stations measured in the 1960s by triangulation and the late 1990s by GPS. We have now realized that these observations were of limited value, because it was difficult to exactly repeat the measured angles and because the angles we could repeat were either very small and thus had small cumulative strains, or were very large but covered areas of low strain. These data are not used here.

2.2.2. Tide Gauge Records

[18] Permanent tide gauge records provide the only continuous measures of deformation since the earthquake, in this case vertical displacement relative to sea level [e.g., *Savage and Plafker*, 1991]. The two preearthquake tide gauges (Seward and Kodiak) were destroyed by the tsunami generated by the earthquake, but were reestablished soon afterward and additional gauges were soon installed. Kodiak, Seldovia, Anchorage, Seward and Cordova provided data starting within the first year after the earthquake, while the Nikiski and Valdez tide gauges were established several years later.

[19] Tide gauges measure sea level relative to land level, and require corrections for eustatic sea level rise as well as seasonal and interannual sea level variations. We used the recent estimate of *Larsen et al.* [2003], which used monthly mean tide level estimates corrected for site-specific seasonal variations and regionally coherent interannual sea level variations (Figure S2). Most records show significant time-dependent signals, most obvious being the large (~100 cm), long-lived relaxation trend seen in the Kodiak record. Nearly half the uplift at Kodiak occurred prior to 1970, but the present uplift rate remains higher than the preearthquake rate. The Anchorage record shows a prominent sinusoidal variation in the first several years after the earthquake; the same feature is seen at Seward but with much smaller amplitude. Repeated leveling surveys made at these tide gauge sites show that these variations are not due to local instability, and are probably real deformation signals of some sort [*Larsen et al.*, 2003]. Because the sinusoidal pattern is not seen at Seldovia, which lies on the water connection between Seward and Anchorage, an oceanographic explanation is unlikely.

2.2.3. Present Velocity Field

[20] The present horizontal velocity field used in this paper is the recently published compilation of *Freymueller et al.* [2008], with small modifications (Figure S3). That compilation combined two separate velocity solutions, one entirely before the 2002 Denali fault earthquake (1993–2002), and a second spanning the time of the earthquake but including a coseismic correction (1993–2007). We found that for a few stations that had significant postseismic deformation following the earthquake, the second solution was used by mistake; we use only the preearthquake solutions for these sites. We also found that for sites in the upper Cook Inlet area, which were affected by a large 1998–2001 slow slip event [*Ohta et al.*, 2006], the 1993–2002 velocities were more self-consistent due to heterogeneous sampling in time, and we used the preearthquake velocities for these sites as well. Our velocity field includes the sites used by other groups who have worked in Alaska, including the data used by *Savage et al.* [1998, 1999] and *Sauber et al.* [2006]. We removed sites affected by volcanic deformation at Augustine, Aniakchak and Veniaminof volcanoes, and used a total of 288 horizontal velocities.

[21] We analyzed all data presented in this paper using the GIPSY/OASIS II software developed at the Jet Propulsion Laboratory (JPL) [*Gregorius*, 1996; *Zumberge et al.*, 1997]. We estimated loosely constrained solutions from each day's data, and then transformed each daily solution into the International Terrestrial Reference Frame 2000 (ITRF2000) reference frame, using the IGb00 realization. Details of the data analysis are given by *Freymueller et al.* [2008].

[22] The general character of the present velocity field remains as described by *Freymueller et al.* [2000] and *Zweck et al.* [2002a]. Near the coast there is a strong along-strike gradient in velocities, from high velocities in Prince William Sound to nearly zero velocities on the Pacific coast of the western Kenai Peninsula. Farther from the trench, sites move in a trenchward direction, opposite to the coastal velocities and opposite to the expected direction from interseismic elastic strain. *Freymueller et al.* [2000] explained these variations as the superposition of a trenchward postseismic deformation signal and interseismic elas-

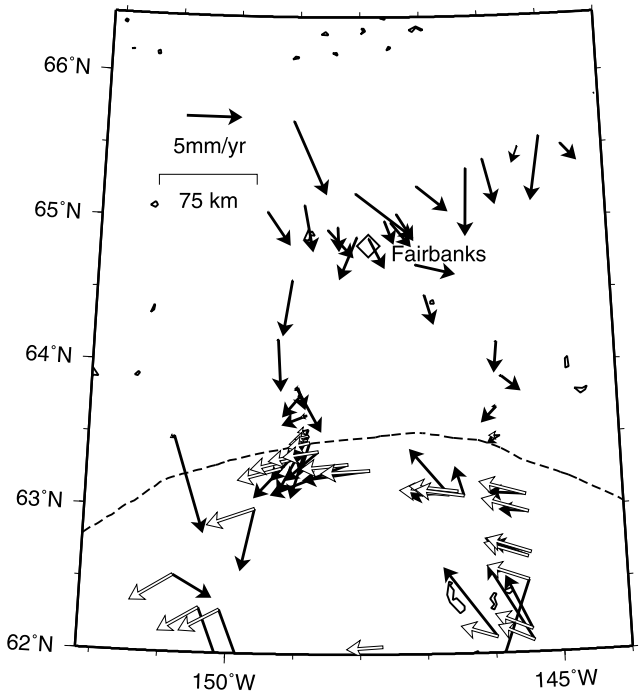

Figure 5. Observed present-day velocities (1997–2007) in Fairbanks area [*Freymueller et al.*, 2008]. Thick dashed lines indicate trace of inland faults. The predicted motions from the southern Alaska block rotation model of *Fletcher* [2002] are shown by white vectors. (See also Figure S3 for across the entire region.)

tic strain from the slip deficit on a locked subduction thrust, where the downdip width of the locked zone varies dramatically along strike. The pattern is somewhat different at Kodiak Island. Along-strike variations are smaller or nonexistent at Kodiak Island, and small trenchward velocities are observed only at sites on the Alaska Peninsula, inboard of Kodiak Island. *Zweck et al.* [2002b] showed that the locked regions corresponded to the regions of high slip in the 1964 earthquake, which led them to suggest that these represented persistent asperities. The spatial resolution of the *Zweck et al.* [2002b] model was very limited at Kodiak Island due to a lack of data, but *Sauber et al.* [2006] used a better data set to show that a significant slip deficit is accumulating offshore of all of Kodiak Island, and a partially locked zone might extend to much greater depth.

[23] Inland from the Kenai Peninsula, the velocity field also shows a complex pattern that results from a superposition of slip on the Denali fault and block rotation [*Fletcher*, 2002] with postseismic deformation and interseismic elastic strain from the subduction zone (Figure 5). Far inland, near Fairbanks and to the north, the small postseismic deformation signal is dominant. There, sites move slowly (2–3 mm/yr) to the SSE relative to North America.

[24] Although we use a single velocity for each site here, site motion is not linear in time over this entire region. *Ohta et al.* [2006] showed that data from sites near Anchorage experienced a significant deviation from linear motion due to a large and long-lasting (2–3 years) slow slip event on the plate interface. The total deformation from the slow slip event is well constrained, but *Ohta et al.* [2006] had data from only one good continuous GPS site, which was installed after the slow slip event began, and they did not develop a time history for the event. The velocities used here average over the time periods before, during and after the slow slip event, and we used the same measurement history at these sites to the extent possible. We used only preearthquake data from sites likely to be affected by postseismic deformation from the 2002 Denali Fault Earthquake.

3. Finite Element Method Description

[25] We used a finite element method (FEM) to compute both the coseismic displacements and the following postseismic deformations caused by the 1964 Alaska earthquake around southern Alaska, using the 3-D FEM code GeoFEM developed at the Research Organization for Information Science and Technology (RIST) [e.g., *Okuda and Yagawa*, 2001; *Iizuka et al.*, 2002]. Complex boundary shapes and internal variations of material properties can be easily handled by the FEM, so this method is suitable for problems where heterogeneities and complex geometries play an important role. 3-D material property variation is a minor effect for the coseismic displacements, considering their uncertainties, but is of critical importance for the postseismic displacements [*Yoshioka and Suzuki*, 1999; *Pollitz et al.*, 2008; *Wang*, 2007]. Our model includes a dipping elastic slab, which profoundly alters the mantle flow and resulting viscoelastic postseismic deformation.

[26] Figure 6 shows the finite element meshes at the surface and a vertical profile along the line A–B. The model mesh is 2000 km long, 2100 km wide, and extends from the Earth's surface down to a depth of 500 km, with 376,831 nodes and 360,000 elements. Our model is composed of an elastic overriding plate and subducting plate, plus a linear (Maxwell) viscoelastic upper mantle wedge and mantle beneath the slab. The low dip angle requires the mesh to be very fine near the fault to maintain suitable element shapes, and the large coseismic stresses require elements to be small near the downdip end of the rupture to avoid numerical imprecision. Table 1 tabulates the material properties assigned to each region shown in Figure 6, taken from *Cohen* [1996] except for the value of viscosity. The thicknesses of the overriding and subducting plates are assumed to be 30 km and 90 km, respectively. We constructed the geometry of the plate interface using the combined plate interface depth contours and profiles of *Doser et al.* [1999], *Page et al.* [1991], *Wolf et al.* [1991], and *Moore et al.* [1991]. Beneath the eastern Kenai Peninsula and western Prince William Sound, the dip of the subducting Pacific plate is very shallow, 3–4.5°, and beneath Kodiak Island 300 km to the southwest, the dip of the subduction interface is 7–9°. Earlier models for the Kenai Peninsula [e.g., *Cohen et al.*, 1995] used a much steeper slab dip angle. The dip angle we used for Kodiak is slightly shallower than that used by *Sauber et al.* [2006].

[27] Boundary conditions are also shown in Figure 6. Taking the X, Y and Z coordinates as indicated in Figure 6, we assume that the model surface is a free surface and the other five outer boundaries normal to the X, Y or Z axes can freely slip only in the Y–Z, X–Z or X–Y planes, respectively. We use the split node technique of *Melosh and*

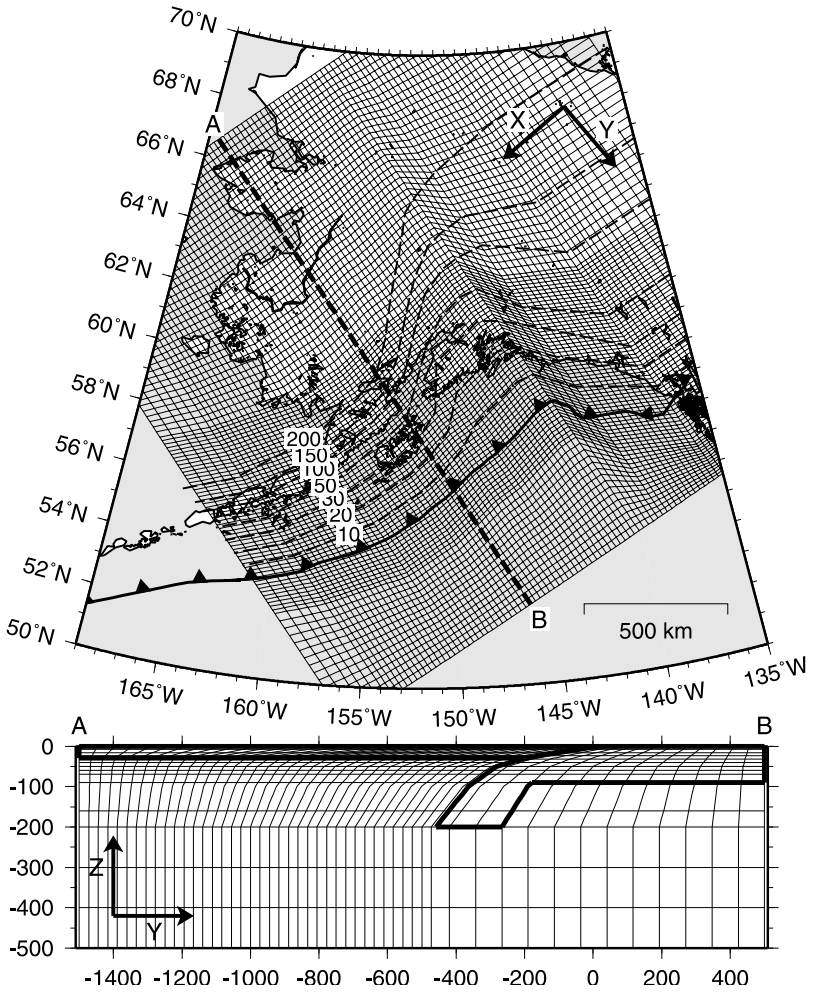

Figure 6. FEM model mesh, illustrating geometry. (top) Barbed lines and dashed thin lines represent the plate boundaries and the isodepth contours of the upper boundary of the subducting Pacific plate, respectively. The thick dashed line shows location of vertical profile A–B in Figure 6 (bottom). (bottom) The area outlined by thick lines represents elastic overriding and subducting plate. The other portion represents viscoelastic upper mantle. Not all the elements are shown in Figure 6 (bottom) for clarity.

Raefsky [1981] to represent slipping faults within the model continuum. This technique induces no net forces or moments on the finite element grid.

4. Coseismic Model

4.1. Modeling Strategy

[28] We refine previously published coseismic slip models in order to make the most precise predictions of postseismic deformation. The models of *Holdahl and Sauber* [1994] and *Johnson et al.* [1996] use the most compatible model geometry, and we use these as the initial basis for our model. After mapping the model of *Johnson et al.* [1996] onto our model geometry, we adjusted the model based on critical reinterpretations of the coseismic displacement data. We also examined in detail the evidence for splay faulting in the upper plate, and we used forward modeling to determine the range of possible models.

[29] The final model (Figure 7) is not based on an inversion, but uses earlier inversion models along with the most critical features of the observations. We then perturbed the model to evaluate the effect of different assumptions on the postseismic model predictions. Inversion of the coseismic displacements is tricky because of the uneven geographical distribution of data, systematic errors, and inconsistencies between some data. Inversions of poorly distributed, inconsistent data subject to systematic errors tend to be controlled by assumed data weights and assumed model smoothing. We preferred to use forward modeling instead to identify which features of coseismic slip are not well constrained and to determine the range of plausible models. Although we developed our model independently, the distribution of slip on the megathrust in our final

Table 1. Material Properties Assigned to Each Region

	Rigidity (GPa)	Poisson's Ratio	Viscosity (Pa s)	Relaxation Time (years)	Type
Overriding plate	50	0.25	–	–	Elastic
Upper mantle	50	0.25	3.2×10^{19}	20	Maxwell
Subducting plate	50	0.25	–	–	Elastic

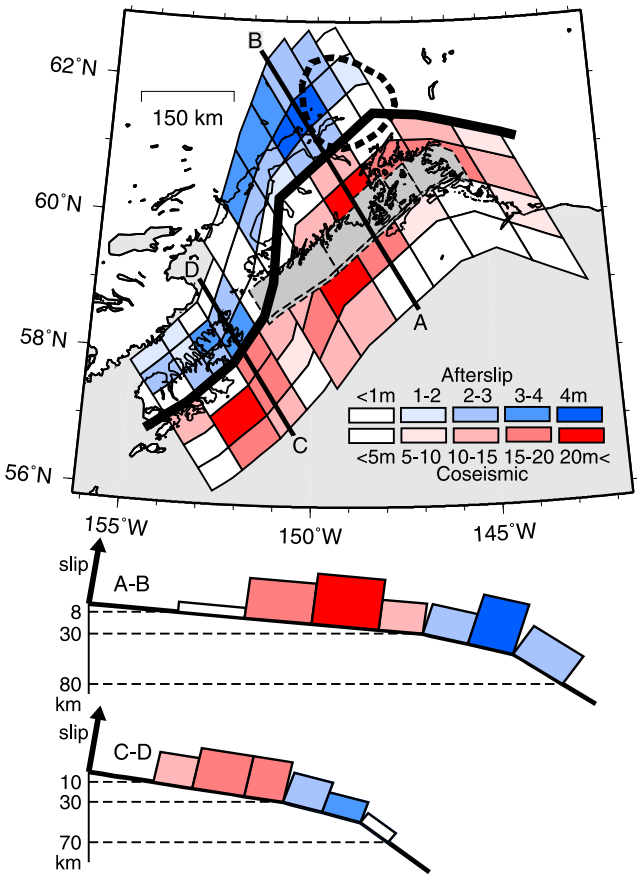

Figure 7. Fault geometry and estimated coseismic slip and afterslip distributions. (top) A thick line separates the area of coseismic slip from the area of afterslip; note that a different scale is used for the two periods of slip. The dashed thick line denotes the area of slow slip event (SSE) reported by *Ohta et al.* [2006]. The shaded areas denote the assumed high-angle splay fault, which extends from Montague Island (where it is exposed) along the length of the Kenai Peninsula. (bottom) Cross sections across A–B and C–D in Figure 7 (top). Note that a different scale is also used for the two periods of slip.

model strongly resembles the recently published teleseismic/tsunami/geodetic inversion model of *Ichinose et al.* [2007].

[30] In sections 4.2 and 4.3, we discuss the horizontal and vertical displacements, and the critical features in these displacements that we used to constrain the coseismic model, relative to previous models. We follow this with an overall comparison of models. Coseismic displacements predicted by our model are shown along with the observations in Figures 2 and 3.

4.2. Horizontal Displacements

[31] Horizontal displacements are available for the eastern half of the rupture zone only [*Parkin*, 1972; *Snay et al.*, 1987]. Thus, constraints on the slip in the Kodiak asperity come from vertical data only. As discussed in section 2.1.1 (see also Text S1), the two critical features of the horizontal displacement field are the along-strike contrast in displacements on the Kenai Peninsula, and the fan-shaped displacement pattern.

[32] The along-strike contrast in displacement requires along-strike variation in the slip on the megathrust. A comparison of the displacements at the western Kenai sites with sites a similar distance from the trench in the eastern Kenai Peninsula or Prince William Sound shows that the displacements were considerably smaller in the western section (Figure 2). This can be explained by a significant reduction in slip and/or reduction in the width of the region that slipped in the west, compared to the east. Present GPS velocities (Figure S3) show a similar contrast, implying a dramatic change in the properties of the plate interface along strike [*Zweck et al.*, 2002a; *Freymueller et al.*, 2008].

[33] The fan-shaped displacement vector pattern can only be explained by a change in rake on the fault plane. The rotation of coseismic displacement vectors through this region strikingly mimics the rotation of present-day GPS velocities [*Cohen and Freymueller*, 2004; *Freymueller et al.*, 2008]. In eastern Prince William Sound, the coseismic displacement vectors are roughly antiparallel to the convergence direction between the Yakutat block and North America [*Fletcher and Freymueller*, 2003], while on the eastern Kenai Peninsula the displacement vectors are roughly antiparallel to the Pacific–North America convergence direction. *Brocher et al.* [1994] and *von Huene et al.* [1999] suggested that the 1964 earthquake involved slip on both the Yakutat–North America and Pacific–North America interfaces, and the coseismic displacements support this hypothesis. We do not model two separate interfaces, but instead approximate the effect by adjusting the rake vector to vary between the Yakutat–North America convergence direction in the east and the Pacific–North America convergence direction in the west. *Holdahl and Sauber* [1994] and *Johnson et al.* [1996] allowed the rake to vary for the Prince William Sound area, but assumed constant rake for the Kodiak segment. Our model has a rake of 90–100° in eastern PWS, and 75–90° from the Kenai Peninsula to Kodiak Island. *Ichinose et al.* [2007] estimated a similar change of rake from teleseismic data.

[34] The model fits the two critical features of the data well, and most of the displacement vectors reasonably well (Figure 2). The model underpredicts the maximum displacements in PWS, but cannot fit them better without violating the vertical displacement data. Scale errors in these displacements could be as large as a few meters, so this misfit may be simply due to scale errors. The model explains the displacements along the triangulation traverse that extends eastward from Fishhook only approximately. These sites are far from the main slip zone, and it is difficult to generate such a displacement gradient with any slip distribution; the misfit probably results from a residual systematic error in the network orientation assumption, and is only marginally significant in any case.

4.3. Vertical Displacements

[35] The oceanward portion of the zero uplift contour passes near the southern edge of Kodiak Island, south of most of the Kenai Peninsula and near Valdez. Cordova, Montague Island, and much of the Gulf of Alaska are in the region of coseismic uplift (Figure 3). The maximum coseismic uplift is around 10 m on Montague Island, due to slip on the Patton Bay high-angle splay fault. Most of Kodiak and Afognak Islands, the Kenai Peninsula and the region

north of Prince William Sound are in the zone of coseismic subsidence. The maximum coseismic subsidence occurred on the northeast portion of Kodiak Island, along the east central portion of the Kenai Peninsula, and at the eastern end of the Turnagain Arm of Cook Inlet. Notably, there is no significant change in the magnitude of the coseismic subsidence along the Pacific coast of the Kenai Peninsula. The effect of that subsidence is still clearly visible today through a series of "ghost forests," stands of trees near the waterline that were killed in 1964 when subsidence brought them into the saltwater tidal zone. The slip model of *Ichinose et al.* [2007] does not predict uniform subsidence along the Kenai coast, and it is difficult to produce such uniform subsidence by slip on the megathrust, especially when that slip must vary along strike in order to explain observed horizontal displacements. The width of the subsidence region broadens considerably around Anchorage. The maximum coseismic subsidence is around 2 m. The positions of the zero line (transition from seaward uplift to landward subsidence) and the axis of maximum subsidence constrain the position of the zone of slip on the megathrust, and the magnitude of the maximum subsidence constrains the slip magnitude.

[36] One of the most spectacular surface manifestations of the earthquake was the ~10 m uplift on Montague Island in Prince William Sound caused by slip on a high-angle splay fault [*Plafker*, 1972]. *Holdahl and Sauber* [1994] and *Johnson et al.* [1996] included this fault, but assumed that the along-strike extent of the fault was limited to a small area, where it is known from its subaerial outcrop. However, the very high slip on this fault suggests it may have a considerably longer length. The pattern of subsidence along the southern (Pacific) coast of the Kenai Peninsula (Figure 3) offers evidence that the splay fault continues offshore along much of the Kenai Peninsula coast. The horizontal data require a large drop in the slip magnitude on the megathrust about halfway between Montague Island and the end of the Kenai Peninsula, but there is no corresponding change in the vertical displacements. Slip on a high-angle fault produces a narrow band of large subsidence on its northwest side, in exactly the right position to explain the subsidence along the coast. Subsidence from slip on the megathrust is centered farther inland (Figure 3). To explain the subsidence along the Kenai coast without a slip on a splay fault, slip on the megathrust would have to be ~30 m, which would significantly overpredict the subsidence elsewhere, and also the horizontal displacements.

4.4. Comparison With the Previous Fault Models

[37] Our slip model strongly resembles those of *Holdahl and Sauber* [1994] and *Johnson et al.* [1996], on which it was based. The main differences are the extension of the Patton Bay fault, and that we find slightly higher slip near the downdip end of the rupture. The largest moment release occurred offshore and beneath Prince William Sound and the eastern Kenai Peninsula, with in excess of 20 m of slip (Figure 7). A smaller asperity beneath Kodiak Island also ruptured with ~20 m of slip, but less slip occurred in the area between these two asperities. Although the Patton Bay fault slipped ~10 m at the southwestern tip of Montague Island, there has yet to be a comprehensive submarine survey that would document the extent of that splay fault. *Holdahl and Sauber* [1994] assumed that the extent of the splay fault was not much larger than its subaerial outcrop on Montague Island. While it will require detailed submarine mapping to test our hypothesis, the results of our forward modeling support extending this splay fault as far as the western end of the Kenai Peninsula.

[38] Total seismic moment of the earthquake, based on our slip model is 7.7×10^{22} Nm, using a rigidity of 50 GPa. This value is slightly higher than past models, 6.3×10^{22} Nm (rigidity of 40 GPa was assumed) [*Johnson et al.*, 1996], 5.0×10^{22} Nm (rigidity of 30 GPa was assumed) [*Holdahl and Sauber*, 1994] and 5.52×10^{22} Nm (assumed rigidity was not reported, but the values given by *Ichinose et al.* [2007, Table 3] show it was ~60 GPa) [*Ichinose et al.*, 2007]. But this difference comes from the assumed value of rigidity.

5. Viscoelastic Model

[39] The viscoelastic postseismic deformation depends on the stress changes from the earthquake, and flow in the viscoelastic medium is fastest where the coseismic stress changes are the largest. The pattern of mantle flow and the surface displacements that result are strongly sensitive to the position and shape of the viscoelastic mantle wedge, which is why a 3-D model including a dipping slab results in such different displacements from a layered model. In the case of southern Alaska region, viscoelastic relaxation produces larger cumulative uplift at Kodiak than in the Kenai Peninsula because of the size of the viscoelastic upper mantle wedge, and its position relative to the slip on the interface. The dip angle of subducting slab becomes gradually steeper from east to west (the Kenai region to the Kodiak region). Because of the steeper dip angle, areas of large slip also extended closer to the wedge in the case of Kodiak. The larger viscoelastic upper mantle wedge and larger coseismic stress changes in the wedge in the Kodiak region result in larger displacements from viscoelastic relaxation. In general, viscoelastic relaxation will cause sites to move toward the trench, with the peak of the trenchward motion located landward of the downdip end of coseismic slip. In the case of the 1964 Alaska earthquake, the slab remains in contact with the overriding plate lithosphere over the entire rupture zone, and the presence of the slab restricts the size of the viscoelastic mantle wedge (Figure 6). Trenchward of this point, the viscoelastic displacements are small because viscous flow is restricted to the mantle beneath the slab, where the stress changes are much smaller and the impact of flow on surface deformation also much smaller.

[40] Given that the model geometry and the coseismic slip model are fixed, the main adjustable parameter in the viscoelastic model is the upper mantle (asthenosphere) viscosity. We computed deformation models using a range of mantle viscosities (η: 1.6×10^{18} to 7.9×10^{19} Pa s), equivalent to Maxwell relaxation times ($\tau = \eta/\mu$: μ is the rigidity, assumed to be 50 GPa) of 1 year to 50 years. The relaxation is not complete during the first 40 years, so all viscoelastic models predict significant displacements today, and the predicted present velocities increase in magnitude as the relaxation time is reduced (assuming $\tau \geq 5$ years). Afterslip on the deeper fault plane following the earthquake

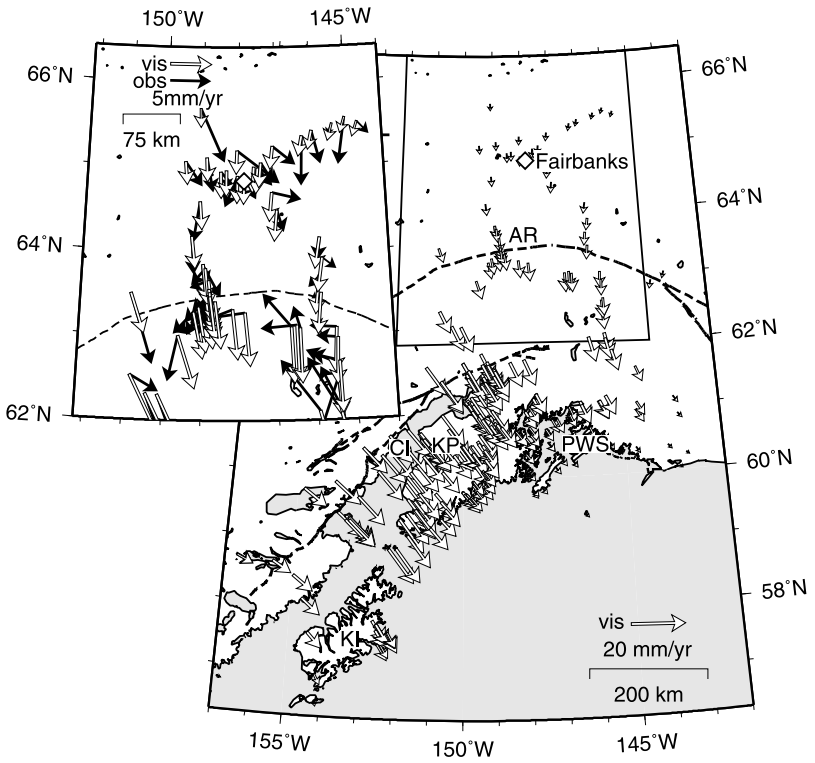

Figure 8. Computed present velocities caused by viscoelastic response. The observations are not shown here for clarity, as they include a large interseismic elastic strain component. Dashed lines indicate trace of inland faults. AR, Alaska Range; CI, Cook Inlet; KI, Kodiak Islands; KP, Kenai Peninsula; PWS, Prince William Sound. The inset shows the boxed region with an expanded velocity scale, along with the observations. Interseismic elastic deformation from the locked subduction zone, and deformation from crustal faults like the Denali fault, are still included in the observations.

will modify the viscoelastic relaxation, because it acts to transfer stress deeper into the mantle. This effect is small compared to the effect of the coseismic model, but it is not insignificant. First, however, we consider only models with no afterslip.

[41] In this section, we show the results of viscoelastic relaxation with a relaxation time of 20 years, our base model (Figures 4, 8, S2, and S4a). This is the relaxation time we consider to be the best fit to the data considering both the cumulative vertical data and present velocities. Here we describe the model and compare its predictions to the cumulative uplift data. We also discuss the dependence of the postseismic model on the coseismic model, and finally we compare the viscoelastic uplift history with the tide gauge time series. In sections 6 and 7 we will introduce afterslip to the postseismic model, and discuss the present velocities and the interseismic elastic slip deficit model needed to explain the present velocities. In sections 6 and 7 we discuss the comparison to the data and how that varies by changing the relaxation time, and the reasons for choosing our base model in more detail.

5.1. Cumulative Uplift

[42] Postseismic uplift is predicted over most of the region that subsided coseismically, but the predicted uplift from viscoelastic relaxation alone is much smaller than the observed uplift (Figures 4 and S4a). Uplift is concentrated slightly downdip of the major slip patches and near the edges of the two main asperities. These are the regions where there are large coseismic stress changes within the viscoelastic mantle wedge. The details of the viscoelastic relaxation are sensitive to the coseismic slip, especially at its downdip end, but the overall observation that the viscoelastic uplift is small compared to the observed uplift does not change unless the coseismic slip at depth is made several times as large as we assume in our model. Predicted cumulative uplift increases as the relaxation time is reduced, but remains less than 40% of the observed uplift even for $\tau = 10$ yr, a relaxation time that is a poor fit to the present velocities. The spatial pattern of the predicted uplift does not change significantly as τ is changed, only the magnitude of the uplift.

[43] At the locations where we have data, predicted uplift from viscoelastic relaxation is small compared to the observed postseismic uplift. On Kodiak Island, predicted uplift from viscoelastic relaxation is 15–40% of the observed total uplift at the western side of Kodiak Island, and less than 15% at the eastern side of the island (Figure 4b). Around the Prince William Sound asperity, the largest predicted uplifts are along the coast of Cook Inlet in the western Kenai Peninsula, but the predicted uplifts are never more than 30% of the observed, and over most of the region the viscoelastic predictions are only 10–20% of the observed (Figure 4a). The peak of predicted viscoelastic uplift lies farther from the trench than the peak of the observed uplift (Figure S4a).

[44] Previous viscoelastic models for the Cook Inlet region [e.g., *Cohen*, 1996] predicted postseismic subsidence in the Kenai Peninsula and Kodiak region, opposite in sign to the observations. This was primarily because those models assumed a dip angle for the subducting slab that was too large. In this case the location of the peaks of postseismic uplift and subsidence are both shifted trenchward from their correct locations.

[45] Clearly, viscoelastic relaxation alone cannot explain the cumulative postseismic uplift on the Kenai Peninsula and Kodiak Island. Changing the relaxation time τ from 20 years to any other reasonable value has only a small effect on the residuals when the model predictions are subtracted from the observations. However, the residual cumulative uplifts are easily explained by afterslip (see section 6).

[46] *Sauber et al.* [2006] reached the same conclusion from their study of Kodiak Island. *Gilpin et al.* [1994] and *Gilpin* [1995] modeled the repeated tidal benchmark surveys they collected using elastic dislocation models, and estimated ~3 m of afterslip over 29 years on a deeper extension of the coseismic fault plane. *Sauber et al.* [2006] included this afterslip in their 2-D viscoelastic FEM, and showed that Gilpin's afterslip estimate provided a good fit to the cumulative uplift data from Kodiak, including the effects of viscoelasticity. This implies that the contribution of viscoelastic relaxation to the cumulative uplift was small.

5.2. Present Velocities

[47] The observed present velocities are not typical of the interseismic period even though more than 40 years have passed since the great earthquake occurred. This is especially obvious on the western part of the Kenai Peninsula and the opposite side of Cook Inlet (Figure S3), where interseismic elastic strain from the locked subduction zone is minimal due to low slip deficit on the plate interface [*Freymueller et al.*, 2000; *Zweck et al.*, 2002a], and the observed velocities are oriented trenchward at a rate of 15–20 mm/yr. Because other contributions to the present velocities are relatively small in this area [*Zweck et al.*, 2002a], and also in the extreme far field near Fairbanks, a comparison of these data to the postseismic models is especially illustrative. Here we describe the general pattern of the present deformation from viscoelastic relaxation; a quantitative comparison will be made in section 7, where we also consider the other effects that contribute significantly to the present velocities, including the interseismic elastic deformation from the slip deficit of the locked seismogenic zone, the rotation of Southern Alaska and slip on the Denali fault [*Lahr and Plafker*, 1980; *Fletcher*, 2002].

[48] Our viscoelastic model predicts trenchward velocities extending the entire length of the earthquake rupture zone (Figure 8). Significant deformation does not extend far in the along-strike direction, but significant viscoelastic deformation extends several hundred km inland from the coseismic rupture zone. *Piersanti et al.* [1997] assumed a dip angle for the coseismic rupture of 20°, far too steep, so the specifics of their model are not correct. However, our improved model supports their conclusion that the 1964 earthquake still produces far-reaching postseismic deformation, at a rate of a few mm/yr. In the Fairbanks area, ~400 km inland from the downdip end of the coseismic rupture and ~650 km inland from the trench, the base model predicts trenchward motion of ~3 mm/yr. Around the Alaska Range (AR in Figure 8), ~200 km inland from the downdip end of the coseismic rupture, trenchward velocities are ~6 mm/yr. In Cook Inlet (CI), a short distance inland from the downdip end of the coseismic rupture, trenchward velocities are ~15 mm/yr. Trenchward velocities decrease at distances closer to the trench.

[49] Thus, even 40 years after the earthquake, the present-day velocities contain a significant component of postseismic viscoelastic relaxation, which produces trenchward motion and uplift. Similar deformations are observed by GPS and are modeled by *Hu et al.* [2004] for postseismic deformation of the 1960 Chile earthquake. Most if not all of the trenchward motion in the Cook Inlet region, first observed by *Cohen and Freymueller* [1997] and modeled in terms of afterslip by *Freymueller et al.* [2000] and *Zweck et al.* [2002a], can be explained as resulting from viscoelastic relaxation. *Ohta et al.* [2006] showed that when our base viscoelastic model is subtracted from the observations, the estimated region of slip deficit on the plate interface (locked region) grows in the downdip direction compared to the estimate of *Zweck et al.* [2002a], although the inference of along-strike variations in the locked region is not changed.

5.3. Dependency on the Coseismic Model

[50] We computed model predictions for several alternate coseismic models, including the previously published models, to evaluate how sensitive the model predictions were to details of the coseismic model. Postseismic model predictions are most sensitive to slip on deeper portion of the fault plane, that is, the slip closest to the viscoelastic material. Plausible slip models do not differ greatly in their deeper slip distribution, so the general pattern of postseismic displacements is similar for all models. Features of the near-field postseismic deformation are more sensitive to changes in the coseismic model than are features of the far-field deformation. For example, the exact location of the peak of cumulative postseismic uplift or the location of the peak present horizontal velocity can be shifted by tens of km by adjusting the coseismic model within reasonable bounds; thus, these features cannot be predicted reliably. However, the rate and orientation of the postseismic model prediction at Fairbanks depends mainly on the total seismic moment of the coseismic rupture rather than details of the slip distribution. In practical terms, uncertainty in the coseismic model is translated into greater uncertainty in the inferred mantle relaxation time.

[51] Our coseismic model assumes that the Patton Bay splay fault extended much further to the west than did previous models [*Holdahl and Sauber*, 1994; *Johnson et al.*, 1996]. On the Kenai Peninsula, the viscoelastic relaxation caused by slip on this splay fault is as large as that for slip on the main thrust in the vertical component. The amount of slip is smaller than that of main thrust, but the steeply dipping fault causes relatively larger vertical postseismic deformations. The splay fault contributes 3–6 cm to the cumulative postseismic uplift in the southern Kenai Peninsula, which for some sites is comparable to the total uplift that results from slip on the megathrust. However, removing the splay fault completely would not change the conclusion

that the total postseismic uplift is dominated by an effect other than viscoelastic relaxation, nor would it alter the present velocity predictions by a significant amount.

5.4. Summary of Viscoelastic Model Compared to Data

[52] Our model predicts that viscoelastic relaxation contributes to the total 30 to 35 years postseismic uplift moderately in the Kodiak region (20–40%), slightly in the western Kenai Peninsula (<20%) and not significantly in the northern Kenai Peninsula (<10%). Therefore, most of the observed total uplift must be explained by afterslip or transient slip. Poroelastic deformation could also contribute, although based on the rapid time decay of poroelastic deformation observed for other earthquakes, it is more likely that this deformation occurred before the first (instrumental) postearthquake measurements.

[53] On the other hand, the viscoelastic model can explain the trenchward component of motion observed in the present velocity field, which *Zweck et al.* [2002a] had previously explained in terms of afterslip. On the western Kenai Peninsula and across Cook Inlet, and in the far field near Fairbanks, where sites are relatively unaffected by other sources of deformation, our base model or alternate models with a relaxation times τ = 15–25 years provides a good match for the observations. *Sauber et al.* [2006] used a slightly longer relaxation time (26 years) for their Kodiak Island model; that value is within the reasonable range.

6. Spatial Distribution and Temporal History of Afterslip

[54] The observed trenchward horizontal velocities far inland from the trench can be explained by the viscoelastic response of the 1964 earthquake (Figure 8), for a relaxation time of 15–25 years. However, the viscoelastic model cannot explain the cumulative postseismic uplift regardless of relaxation time (Figure 4). After removing the viscoelastic response, the largest residual cumulative uplifts are located downdip of the areas of largest coseismic slip, consistent with afterslip as the dominant mechanism for cumulative uplift. Afterslip is reasonably efficient at producing uplift, especially when it occurs on a deeper extension of the coseismic rupture surface that dips more steeply. In this section we model the residual postseismic uplift, which is the cumulative vertical displacements corrected for GIA, interseismic elastic deformation, and the uplift from viscoelastic relaxation.

6.1. Spatial Distribution of Afterslip

[55] Given the along-strike variations in the coseismic slip distribution, we cannot assume that afterslip was uniform along strike. Based on the observed cumulative uplift pattern, afterslip must have been concentrated downdip of the two main slip patches (Figure 7). We assumed that afterslip was located entirely downdip of the coseismic rupture, although it is possible that the deeper segments of the coseismic rupture experienced both coseismic and postseismic slip. The detailed shape of the afterslip region is poorly constrained by data. We modeled the afterslip as having a constant spatial pattern but a rate that varies with time; that is, that the area of afterslip does not migrate spatially with time. This assumption is probably an oversimplification, but it is adequate because only the tide gauge data provide any information on time dependence. We incorporated the viscoelastic response to the imposed afterslip, although this effect is generally less than 10% of the magnitude of the deformation of the afterslip itself.

[56] Figure 7 shows our model afterslip distribution compared with the coseismic slip distribution. The characteristic feature is that large afterslip is located downdip of the areas of large coseismic slip. Our model includes no slip in the deeper part of northeast PWS region and very small slip in the area between the Kenai Peninsula and Kodiak Island, although these aspects of the model are very poorly constrained. Afterslip plausibly could have occurred in these areas, but no data exist to determine whether or not it did (see also section 8.3).

[57] The model fits the residuals (observed minus viscoelastic, glacial rebound and interseismic elastic deformation) very well over most of Kodiak Island and the Kenai Peninsula (Figure 9). The model overpredicts the uplift in the southern Kenai Peninsula, near Seward. Starting on the Pacific coast at Seward, there is a very rapid landward increase in the cumulative uplift over a distance of only 50–100 km, which is difficult to generate with any afterslip distribution. In Kodiak Island, the model also fits the data very well.

6.2. Temporal History of Afterslip

[58] Three tide gauges (Kodiak, Nikiski and Seldovia) show significant postseismic uplift (Figure 10), and the total uplift of all three are significantly underpredicted by viscoelastic relaxation alone, because of the same geometric factors that cause the total uplift to be relatively small: a very shallow fault dip and a small wedge-shaped viscous region mean that postseismic uplift cannot be large. However, after about 1990 the observed uplift rates are similar to those predicted of the viscoelastic model. To explain these data, we need to include an additional component, like afterslip, that produces substantial uplift in the early years after the earthquake but relatively little uplift today. The other tide gauges show a more complex vertical motion history (Figure S2), discussed in section 8.1.1.

[59] Using the afterslip spatial distribution derived in section 6.1, we modeled the afterslip time history by considering three alternative different temporal decay functions: logarithmic, exponential, and Ohmori's Law. Even though these functions have very different forms, with a proper choice of relaxation times all three can produce very similar behavior over a few decades, and the data are not sufficient to distinguish between them. The exponential model produced a slightly better fit, and we modeled the time history using an exponential function ($U_s = A \times (1 - \exp(-dt/T))$), where U_s is the slip as a function of space and time on plate boundary, A is a constant that depends on space, dt is the time since the earthquake, and T is a characteristic time. The constant A includes a normalization factor so that the total afterslip represents slip between 1964 and 2001.

[60] For the Kodiak region, we used magnitude of afterslip from the cumulative postseismic uplift data (Figure 7), about 3 m total afterslip in the peak area, and an exponential relaxation with a characteristic time, T = 10 years (Figure 10a). The model provides an excellent fit to the

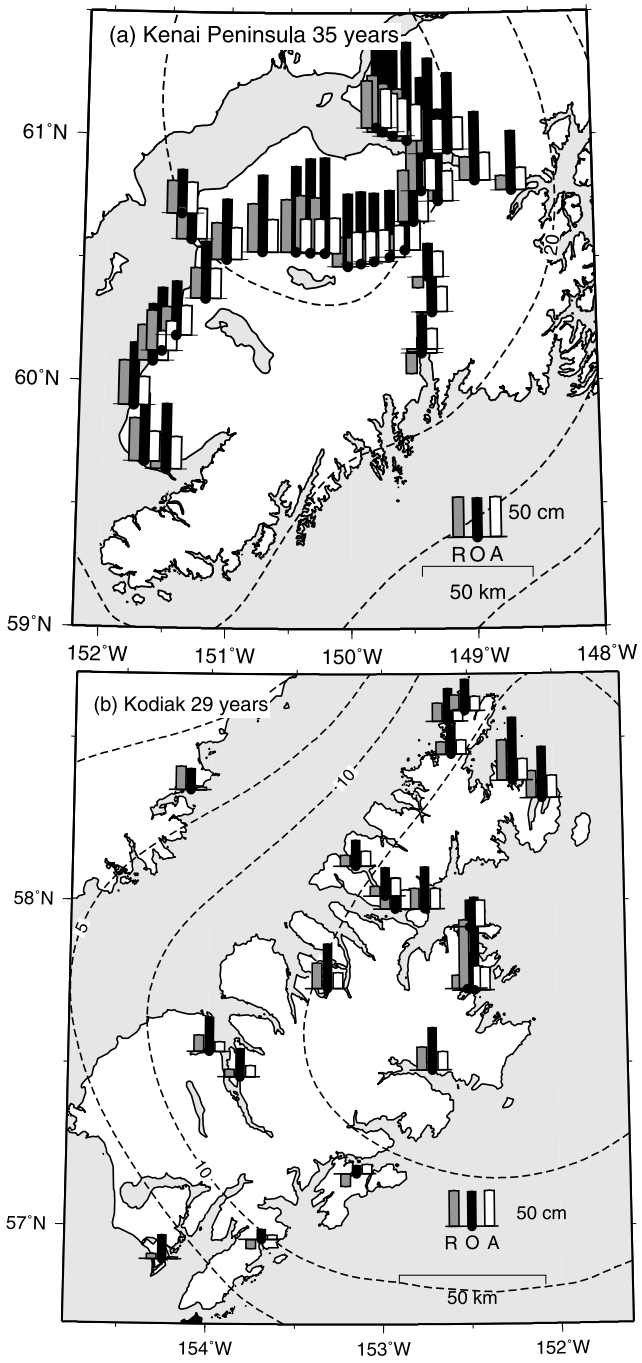

Figure 9. Computed postseismic uplift caused by afterslip. (a) Time span for 35 years in Kenai Peninsula, as compared with the observation at leveling benchmark [*Cohen and Freymueller*, 2004]. (b) Time span for 29 years in Kodiak Island, as compared with the observation at tidal benchmarks [*Gilpin et al.*, 1994; *Gilpin*, 1995]. O, observation; A, afterslip effects; R, residual (observation minus viscoelastic effect, glacial rebound, and interseismic elastic deformation). (See also Figure S4b for across the entire region.)

data, especially when the interseismic elastic deformation is also removed. This model underestimates the extremely rapid uplift in the first few years after the earthquake, which might indicate a more complex time history, or might reflect the impact of an additional postseismic component, perhaps poroelastic relaxation [*Masterlark*, 2003]. For the Cook Inlet and Prince William Sound areas, we adjusted the time history and magnitude of afterslip based on the tide gauge records from the two Cook Inlet sites, Seldovia and Nikiski (Figure 10b). Peak afterslip in this patch is 4 m, slightly larger than the case for Kodiak region. In this model, the initial rate of afterslip at the afterslip peaks is ~30 cm/yr

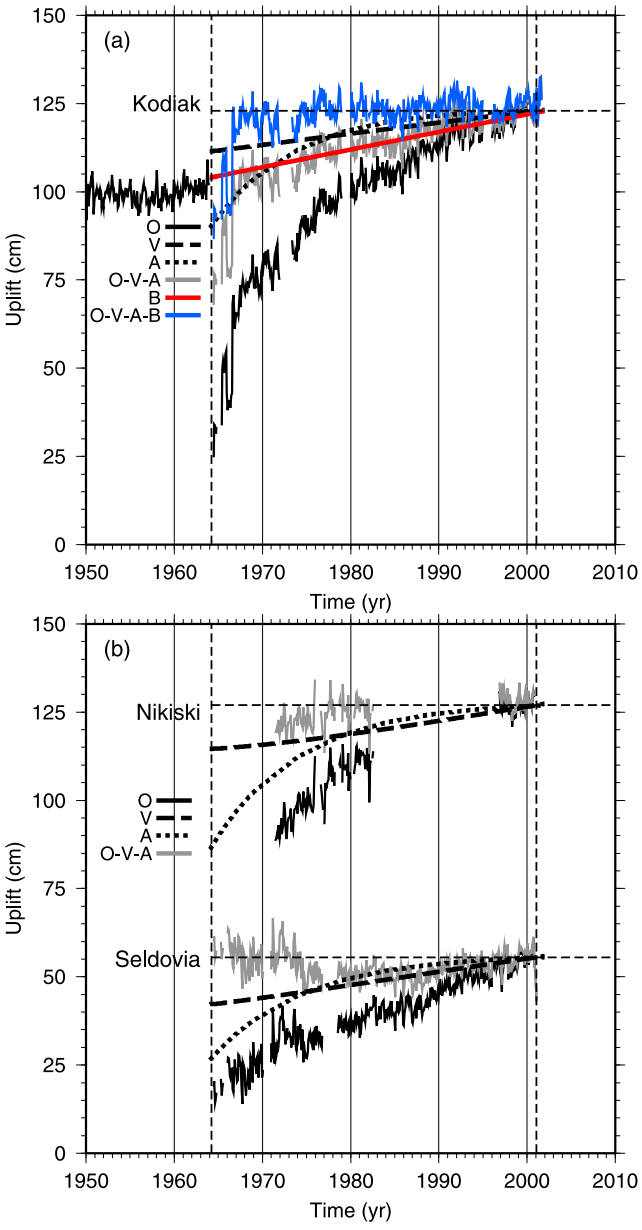

Figure 10. Best fit model (viscoelastic response + afterslip) of uplift history at tidal gauge stations: (a) Kodiak and (b) Nikiski and Seldovia. The locations of tide gauge stations are shown in Figure S4. O, observation; V, viscoelastic effect; A, afterslip effect; O-V-A, observation – viscoelastic effect – afterslip effect. The red line in Figure 10a shows the predicted rate for interseismic elastic deformation, and the blue curve shows the tide gauge data corrected for the interseismic elastic deformation. The other stations, Anchorage, Seward, Valdez, and Cordova, are shown in Figure S2.

immediately after the earthquake, and after 30 years the rate of afterslip has declined to ~1 cm/yr.

7. Interseismic Elastic Deformation

[61] The interseismic elastic deformation in the 1964 rupture zone is both large and variable along strike [*Zweck et al.*, 2002a]. Without including a model for this large deformation component, we can compare the postseismic model only to data from sites in the far field, far enough from the trench that the elastic strain from the interseismic slip deficit is small. By including an interseismic model, we can use additional sites to determine the best viscoelastic relaxation time. We estimate the interseismic slip deficit distribution in these models rather than imposing a model based on thermal models [e.g., *Oleskevich et al.*, 1999], because of the strong lateral variations observed in the data, which are not expected based on thermal modeling [*Freymueller et al.*, 2008].

[62] The present velocities also include a contribution due to motion of southern Alaska relative to North America [*Freymueller et al.*, 2008]. We applied a correction (white vectors in Figure 5) based on the southern Alaska block rotation of model of *Fletcher* [2002; see also *Freymueller et al.*, 2008], which specified a pole of rotation and angular speed for the motion of southern Alaska south of the Denali fault. This pole of rotation in this model was based on the curvature of the trace of the Denali fault [*Stout and Chase*, 1980], and the angular speed by the observed GPS velocities across the Denali fault. We compared interseismic model inversions with and without including this model, and the overall model misfit (over all sites north of 62°N) was reduced by almost a factor of two when this correction is included, compared to an inversion when it is not included (Figure 11). Thus, we only discuss models that include this correction. The data vectors shown in Figure 11 have had the southern Alaska block rotation model subtracted.

7.1. Modeling Approach and Model Evaluation Criteria

[63] For each relaxation time from 5 years to 50 years, we estimated the elastic interseismic slip deficit model after removing the predicted postseismic velocities and southern Alaska block rotation from the data. We defined the present model velocities as the average velocity over the period 1997–2007, which approximates the time span of the GPS data. We used the complete postseismic model, including afterslip model of section 6.

[64] We estimated interseismic models using two different methods. The first method followed that of *Zweck et al.* [2002a]. This inversion method is based on *Harris and Segall* [1987], and incorporates smoothing by estimating the Laplacian of the slip distribution rather than the slip distribution itself. The inversion is computed using the Singular Value Decomposition (SVD), and retaining a larger or smaller number of singular values in the solution varies the degree of smoothing in the model. A larger number of singular values results in a spatially rougher solution. We also used an inversion method with inequality constraints [*Ward and Barrientos*, 1986], which forces the slip deficit to remain less than 100% of relative plate motion. We estimated both a smooth and rough model using SVD inversion, using 15 and 20 singular values, respectively. For comparison, the smooth model applies about the same smoothing as the model of *Zweck et al.* [2002a], and the rough model applies considerably less smoothing, reflecting the improved distribution of data. The differences in predicted deformation between the three models are mainly confined to the region nearest the trench, where the interseismic elastic deformation is the largest, but the smooth model oversmoothes the slip deficit distribution on the Alaska Peninsula and Kodiak Island, and smoothes over the 1998–2001 slow slip event in upper Cook Inlet. As a result, we discuss only the rough SVD model here.

[65] We used a significantly larger model region than *Zweck et al.* [2002a], extending from east of Prince William Sound to the end of the Alaska Peninsula in the west. The slip deficit distribution along the Alaska Peninsula was modeled previously by *Fournier and Freymueller* [2007] and *Cross and Freymueller* [2007], and details of the model outside the area of the 1964 rupture zone will not be discussed here. We used the complete data set of Figures 5 and S3 in all inversions, and weighted the data based on their uncertainties. We did not include correlations between sites or between the horizontal components in the data weighting.

[66] Because we estimated the extent of the zone of interseismic slip deficit, we found that there were very strong tradeoffs between the viscoelastic model and the interseismic model, even for sites as far from the trench as Cook Inlet. If the trenchward motion in the postseismic model is reduced or increased, the interseismic model can compensate for this to a large extent by changing the downdip width of the locked region. This tradeoff breaks down in the far field, because the interseismic models can no longer compensate. Thus, we found that only sites north of 62°N, away from the region of largest interseismic elastic deformation, are diagnostic of the relaxation time.

[67] We evaluated the interseismic models based on two criteria. The first was the weighted sum of squared errors (SSE) over all sites north of 62°N. South of this line, the SSE is dominated by details of the interseismic model for sites where the postseismic correction is small, but interseismic deformation is large. We also evaluated models based on their consistency with the overall temporal history of afterslip (section 6), which predicts that the present rate of afterslip should be small (~1 cm/yr). As in the work by *Zweck et al.* [2002a], we can fit the data reasonably well by applying no postseismic model at all, and in this case we estimate an extensive region of rapid afterslip (several cm/yr) downdip of the coseismic rupture. However, such an approach would be valid only in the case of a purely elastic mantle, because it ignores the viscoelastic response to both the coseismic slip and the more recent afterslip. Any model that fits the present velocities can be rejected if it requires significantly more rapid afterslip at present than the temporal model of section 6.

7.2. Model Results

[68] The best model has a relaxation time of 20 years (Figure 11), considering both evaluation criteria, although any models with relaxation time from 15 to 25 years also produces acceptable results. The interseismic model pre-

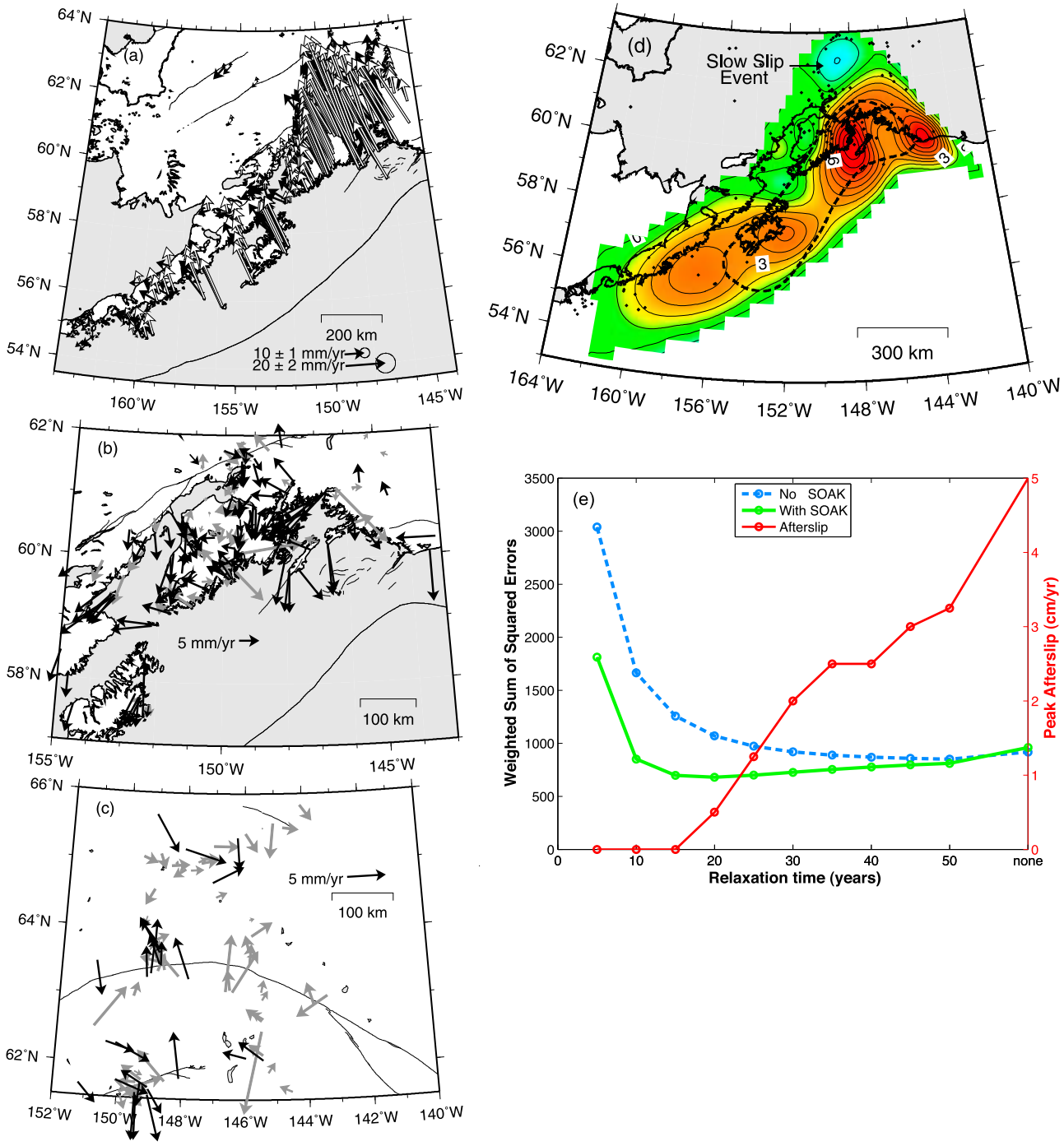

Figure 11. Interseismic elastic deformation models. (a) Data with base postseismic model and southern Alaska block rotation subtracted (black vectors) and model predictions for the interseismic elastic deformation (white vectors). (b) Residuals for the Cook Inlet and Kodiak regions. Gray vectors are sites for which the residual is $<2\sigma$, and black vectors are the sites for which the residual is $>2\sigma$. (c) Residuals for the northern region, with the vector colors meaning the same as in Figure 11b. (d) Interseismic slip deficit model, with contour interval of 1 cm/yr. Red colors are positive slip deficits, and blue colors are negative slip deficits (mainly the effect of the 1998–2001 slow slip event [*Ohta et al.*, 2006]). (e) Weighted sum of squared errors and magnitude of peak afterslip in lower Cook Inlet (NW of Kenai Peninsula) for models with various relaxation times. Solid green curve is for models with southern Alaska rotation model subtracted, and dashed blue curve is for models without this correction. Red curve is magnitude of peak afterslip.

dictions are compared to the corrected data in Figure 11a, and residuals are shown in Figures 11b and 11c. The interseismic slip deficit model itself is shown in Figure 11d. Because we have focused in this paper on the viscoelastic model and not the interseismic model, caution should be applied in interpreting details of the interseismic slip deficit model. For example, a change in the amount of smoothing or the slip boundary conditions at the updip end of the model could make for a large difference in the estimate of the slip deficit in the shallow part of the seismogenic zone. The rounded character of all contours results from the smoothing, and the model is probably oversmoothed in the Alaska Peninsula segment. In the model that uses the method of *Ward and Barrientos* [1986], the megathrust is completely locked out to the trench rather than smoothly decreasing to zero slip deficit as in the model shown. However, the models estimated using this method tended to estimate regions of slip deficit at the deepest part of the model, which are most likely due to unmodeled motions of the upper plate. A more comprehensive discussion of the interseismic slip deficit distribution will be the subject of a forthcoming paper.

[69] Relaxation times of 10 years or less can be eliminated based on their poor fit to the data (Figure 11e). These models predict rapid trenchward motion of the far field sites, at rates much faster than observed. We found that all reasonable slip deficit models predicted elastic deformation of ~1 mm/yr at Fairbanks, so postseismic models that overpredict the trenchward motion there could not fit the data well. The large misfit in these models is not confined only to the far field; the largest reasonable elastic interseismic deformation for sites in the Alaska Range area is 3–4 mm/yr, and postseismic models with a short relaxation time overpredict trenchward velocities here and in Cook Inlet as well.

[70] Models with relaxation times longer than 25 years can be eliminated based on inconsistency with the afterslip history (Figure 11e). Because the predicted postseismic deformation becomes smaller with increasing relaxation time, these models become more and more like the model with no postseismic correction as the relaxation time is increased. However, the interseismic models can only fit the data by including larger and larger rates of present afterslip, which conflicts with the temporal history of afterslip determined from the tide gauge data. The peak present afterslip rate in models with no postseismic correction is ~5 cm/yr, while the peak present afterslip rate in the base model (20 year relaxation time) is ~0.5 cm/yr, a value that agrees with the overall temporal afterslip history.

[71] The residual velocities are dominated by spatially coherent residuals that probably reflect unmodeled motions of the overriding plate relative to North America. For example, most sites in the Cook Inlet region show a southeastward residual of ~5–8 mm/yr, in a trench-parallel direction (Figure 11b). The residuals are roughly orthogonal to both the predicted postseismic deformation and the predicted interseismic elastic deformation, so the trench parallel component does not change much for different postseismic models. Similar trench-parallel residual motions extend across the entire rupture zone, including Kodiak Island (Figures 11a and 11b). These residual motions are very similar to the motion of the Alaska Peninsula estimated by *Cross and Freymueller* [2007], and they suggest that the crust south of the active Castle Mountain–Lake Clark–Bruin Bay faults moves southeast 5–8 mm/yr relative to the block immediately south of the Denali fault. We have already removed a block rotation that explains the motion immediately south of the Denali fault, so the crust here must move even faster relative to North America. Farther north, residuals are small and show no large spatially coherent character (Figure 11c). There are small, local areas of misfit, but these vary from model to model and will not be discussed further. The sites shown in Figure 11c are those used to evaluate the misfit for the purposes of choosing the best viscoelastic model.

[72] The best fitting interseismic elastic model (Figure 11d) resembles the model of *Zweck et al.* [2002a] in general character, but there are some significant differences in detail. First, the estimated region of significant slip deficit in our new model is 20–50 km wider. As discussed in *Freymueller et al.* [2008], this is a consequence of the viscoelastic postseismic deformation being aliased into afterslip in the previous model. Second, our new model suggests that the Prince William Sound asperity may be divided into two distinct parts; the eastern part is east of the area modeled by *Zweck et al.* [2002a]. Finally, the shape of the western edge of the Prince William Sound asperity is somewhat different. The new data we have added from the coastal part of the Kenai Peninsula require the transition from the wide locked region to the east and the narrow or nonexistent locked region to the west to be abrupt. The interseismic model remains somewhat poorly resolved for the Kodiak Island region, due to the lack of data from central Kodiak. Unlike the earlier model, we find a significant locked region extending across all of Kodiak Island, which is consistent with the findings of *Sauber et al.* [2006]. We do not find any clear correlation between the present interseismic slip deficit model and the SE end of the 1964 earthquake rupture. In fact, our model suggests that the locked region may be even wider and slip deficit larger in the 1938 rupture zone to the southeast than in Kodiak Island, although this may be an artifact of smoothing.

8. Discussion

8.1. Relative Importance of Viscoelastic Relaxation and Afterslip

[73] Both afterslip and viscoelastic contributed significantly to the postseismic deformation over the entire 1964 rupture zone, which extends the result of *Sauber et al.* [2006]. *Zweck et al.* [2002b] showed that no single relaxation trend could fit both the early deformation rates observed by leveling and the 30-year cumulative displacements for the Kenai Peninsula. Similarly, our modeling shows that no single mechanism can explain both the 30 to 35 year cumulative displacements and the present velocities, but a combination of viscoelastic relaxation, afterslip and interseismic slip deficit can explain all first-order features of the data.

[74] The results of sections 5–7 highlight an intriguing feature of the available postseismic data sets for the 1964 Alaska earthquake. We have data covering two very different time periods, the ~30-year cumulative uplift and the present-day velocities, and each of these data types is sensitive mainly to one mechanism of postseismic defor-

mation. The cumulative 30-year uplift data are sensitive mainly to afterslip (most of the afterslip occurred in the early part of this period), while the postseismic deformation in the present velocities is dominated by viscoelastic relaxation. This feature of the data sets allowed us to constrain the mechanisms separately and then determine a combined, multimechanism model, including the interseismic elastic deformation from the slip deficit on the megathrust. A nonlinear or transient mantle viscosity would complicate this approach, if the effective viscosity changed by an order of magnitude or more over a large region of the mantle during the first 2–3 decades after the earthquake. That would require the ambient deviatoric stress magnitude in the mantle to be of the order of the coseismic stress change or smaller, for a typical stress exponent n$\sim$3.5 inferred for mantle materials. However, even in this case the cumulative postseismic uplift would be dominated by afterslip because the geometry of the subducting slab allows little viscoelastic uplift. Further exploration of this possibility would require a fully nonlinear model and is beyond the scope of this study.

[75] Our model was optimized to fit the tide gauge records, 30-year postseismic uplift data, and the present velocities in concert with an interseismic slip deficit model. This model is clearly nonunique, and some features of the model can never be constrained by data, because no long-term postseismic data will ever exist from the NW shore of Cook Inlet, for example, or from other critical regions where measurements were not made shortly after the earthquake. Our goal was to identify the critical features of the model that are required by the data.

8.1.1. Tide Gauge Data

[76] We discuss the four remaining tide gauges in regional groups of two, Anchorage and Seward on the eastern Kenai Peninsula (Figure S2c), and Valdez and Cordova in Prince William Sound (Figure S2d; see Figure S4 for locations). For these gauges, we compared the predictions of our model to the observed tide gauge records, rather than using the records to adjust the model. Figure S2 shows the original tide gauge records as a black line, along with the model predictions and residual records after removing the postseismic model (gray curves). For certain sites, we also remove an interseismic elastic correction, and show the final residual record as a blue curve. If the model explained the records fully, the resulting residuals would follow a horizontal line.

[77] The tide gauge records at Anchorage and Seward (Figure S2c) are fit poorly by the model. Both tide gauge records would be fit reasonably well by the viscoelastic model alone. The viscoelastic + afterslip model significantly overpredicts the postseismic uplift at these sites. This is puzzling, given that the region of maximum postseismic uplift ($\sim$1 m) is located between them. We do not know how to explain the Anchorage tide gauge record, except to note that cumulative uplift measurements nearby also do not agree with it, and it is possible that the area around the tide gauge is subsiding for reasons unrelated to the earthquake. The misfit at Seward might result from an erroneous correction for the interseismic elastic deformation, if we have underestimated the width of the locked zone in our correction. If the locked zone was wide enough, Seward would shift from the zone of uplift to the zone of subsidence. Our interseismic models do not show this, but the model of *Ohta et al.* [2006] suggested that this could be the case.

[78] The Valdez and Cordova tide gauge records are explained well by our combined postseismic and interseismic model (Figure S2d). Valdez and Cordova are both located in eastern Prince William Sound, with Cordova located about 65 km trenchward of Valdez. Both sites are located above the locked region on the plate interface, and the tide gauge records include significant contributions from interseismic elastic deformation. The deformation due to afterslip is negligible at these sites, and the deformation due to viscoelastic relaxation is small. The Valdez record corrected by the total postseismic model is explained reasonably well (gray curve in Figure S2d). The interseismic deformation (red line) appears to overcorrect slightly (blue curve), but the trend of the record is still reasonably flat with only a slight residual uplift not explained by the model. This record is one of several that feature a kink around 1990, although it is not clear whether this represents a common mode signal or noise. At Cordova, the interseismic elastic subsidence (red line) is the largest component of the tide gauge record. The record with postseismic and interseismic deformation removed (blue curve) is reasonably flat, but includes a small additional subsidence trend not predicted by the model. In both cases, small adjustments to either the interseismic or postseismic models could explain the remaining signals.

8.1.2. The 30-Year Cumulative Displacements

[79] In Figure 12 we show the contributions from both viscoelastic relaxation and afterslip for the 30-year cumulative displacements. Figures 12a and 12c compare the model predictions to data, while Figures 12b and 12d show the predicted horizontal displacements from the model. There are no cumulative horizontal data, but the predictions may be used in comparison to other earthquakes.

[80] Afterslip dominates the cumulative vertical motion (Figures 12a and 12c). The sum of the two postseismic components matches the observations well after the interplate coupling and glacial rebound correction, except as noted before. Predicted cumulative horizontal displacements from afterslip are on the order of 0.5–1 m, comparable to the viscoelastic displacements; total horizontal postseismic displacements are predicted to be 1–2 m, with the peak located near Cook Inlet. Toward Seward, the effect of afterslip becomes small, because the afterslip component declines more rapidly in space due to its shallower source. These model predictions cannot be compared to data, but they can be used to predict what might be observed at near-field sites in similar earthquakes, such as the 2004 Sumatra-Andaman earthquake. At near-field sites in the Andaman and Nicobar Islands, the first-year horizontal postseismic deformation reached magnitudes of up to 20 cm, not counting the deformation in the first few weeks after the earthquake [*Freymueller*, 2005]. Over the first two years, horizontal displacements were up to 32 cm, and vertical displacements exceeded 20 cm at some sites [*Paul et al.*, 2007]. The early deformation rate after that earthquake is similar to that predicted by our model for the 1964 Alaska earthquake.

8.1.3. Present Velocities and the Persistence of Afterslip

[81] Figure 13 shows the postseismic model predictions for the present horizontal velocities. Viscoelastic model

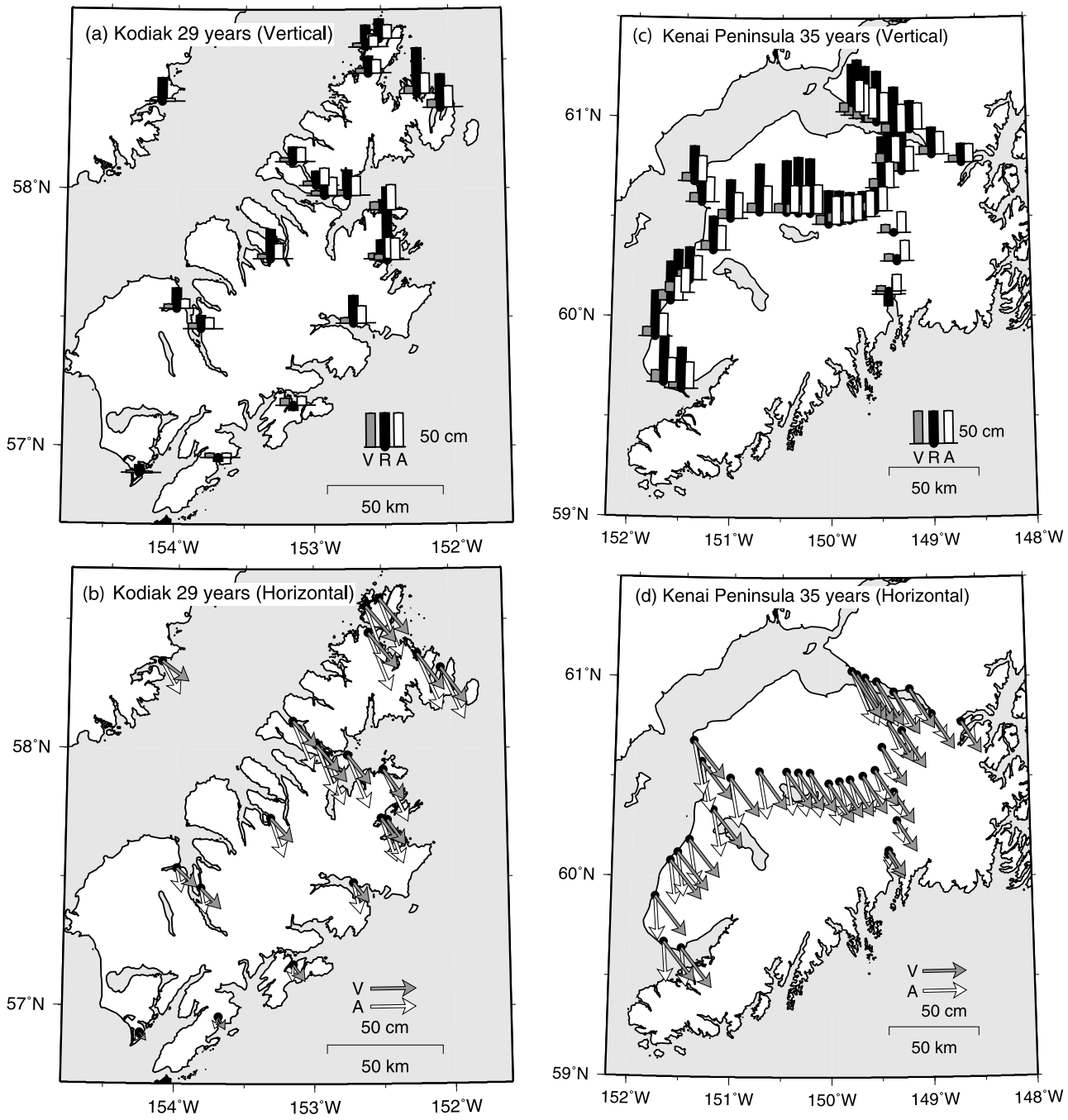

Figure 12. Total uplift for each mechanism, viscoelastic response (gray), and afterslip (white). (a) Vertical and (b) horizontal displacements at Kodiak Island for 29 years. (c) Vertical and (d) horizontal displacements on the Kenai Peninsula for 35 years. There are no 1964–present horizontal postseismic observations, so computed horizontal displacements are shown for comparison to other earthquakes. R, observation minus glacial rebound and interseismic elastic deformation; V, viscoelastic effect; A, afterslip effect.

predictions are trenchward in direction, and increase from 1 to 3 mm/yr north of 65°N (~800 km inland from the trench) to 6–8 mm/yr between 62°N and 63°N (~500 km inland from the trench, or ~150 km inland from the downdip end of coseismic rupture). The maximum velocities from viscoelastic relaxation are located 300–400 km inland from the trench, or slightly inland of the downdip end of coseismic rupture, with a magnitude exceeding 10 mm/yr. At the Pacific coast, which lies over the rupture zone, the viscoelastic model predicts velocities <5 mm/yr.

[82] The magnitude of the afterslip component varies substantially with space, as expected from the spatially variable distribution.

[83] The exponential time decay function we assumed predicts that measurable afterslip still occurs today, 40 years after the earthquake. With the time constants found in this

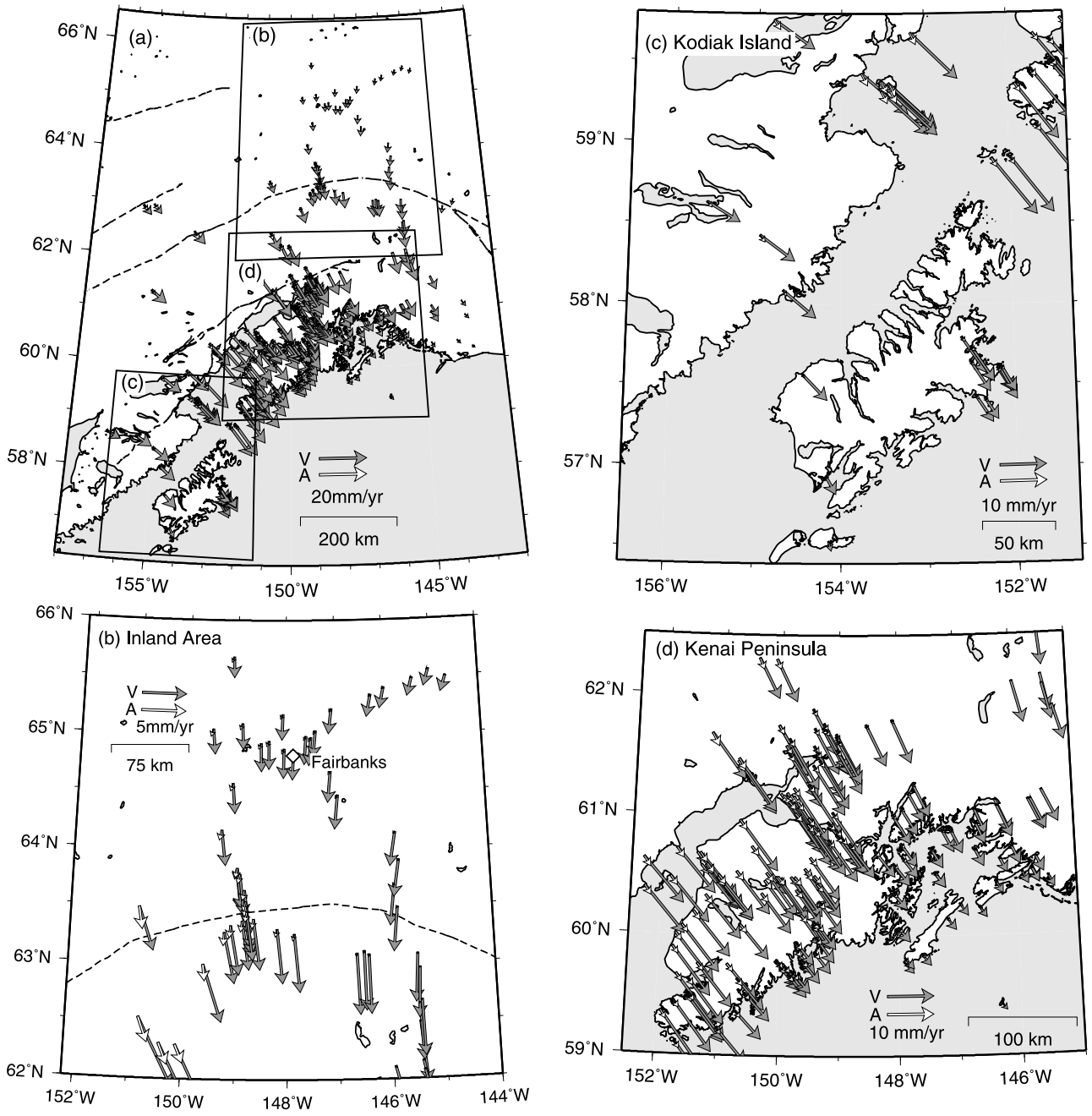

Figure 13. Present velocities (1997–2007) for each mechanism, viscoelastic response (gray), and afterslip (white). (a) Whole region. Dashed lines indicate trace of inland faults. (b) Inland area. Dashed line indicates trace of the Denali fault. (c) Kodiak Island. (d) Kenai Peninsula region.

study (T = 10 years), an exponential time decay model predicts that 95% of the total afterslip will occur within 30 years after the earthquake. However, if the total afterslip is 4 m, this means that 20 cm of afterslip will occur more than 30 years after the earthquake. A logarithmic or Ohmori's Law time decay function predict similar results, for time constants that fit the Kodiak tide gauge record. Our preconceived notion is that afterslip is a short-lived phenomenon, lasting for a few years at most. This notion is based primarily on our experience from M∼7–8 earthquakes, which are tiny in comparison to the giant M9+ ruptures, and may simply reflect the time it takes for the afterslip signal to disappear below the noise level, or to become small compared with longer-lived viscous relaxation. When the rate of postseismic deformation at 1 year after the earthquake is 10–20 cm/yr, even 5–10% of that rate remains significant given the precision of modern measurements.

[84] Rate and state friction models also suggest that afterslip may be very long lived. *Marone et al.* [1991] showed that a rate and state friction law and reasonable approximations lead to logarithmic time decay for the displacements due to afterslip (velocity decays with time according to ∼1/t). *Perfettini et al.* [2005] investigated the coupling between a deep fault zone obeying rate and state

friction (velocity strengthening) and a deeper ductile fault zone with a viscous rheology. Their model predicts that afterslip rate and aftershock rate are linked, and thus afterslip may take a long time to decay to "background" rates. To answer the question of how long afterslip can last, we may need decades of modern data following another M9+ earthquake.

8.2. Width of the Zone of Interseismic Slip Deficit

[85] The postseismic contribution to the present GPS velocities is dominated by the effect of viscoelastic relaxation, which means that past studies of horizontal velocities in the Kenai Peninsula and Cook Inlet area need to be reconsidered. Along-strike variations in the slip deficit distribution are not significantly affected by the correction, but the estimated width of the zone of slip deficit changes substantially. The model of *Zweck et al.* [2002a] underestimated the width of the zone of slip deficit. The shape and downdip extent of the inferred asperities changes after postseismic corrections are applied, although the along-strike variations are not affected.

[86] The zone of interseismic slip deficit on the megathrust is inferred to reach a significantly greater depth after correction for the viscoelastic model [*Ohta et al.*, 2006]. That study considered deformation in two time intervals, before and after a large slow slip event (SSE) on the plate interface, and during the SSE. Before and after the SSE, *Ohta et al.* [2006] estimated that the fully locked region of the plate interface extended ~50–75 km farther downdip than *Zweck et al.* [2002a] estimated for the same time period. However, much of this downdip region slipped during the 1998–2001 SSE, and during the time period of the SSE the downdip of end of the locked zone estimated by *Ohta et al.* [2006] coincides roughly with the downdip end of the aftershock zone estimated right after the earthquake [*Furumoto*, 1965]. This correspondence led *Ohta et al.* [2006] to suggest that part of the plate interface that slipped during the SSE probably failed repeatedly in SSEs, and thus was at a relatively low level of shear stress at the time of the earthquake, insufficient to sustain seismic rupture. In our coseismic slip model, we estimated little or no slip in the region of the SSE, although significant afterslip occurred there (Figure 7).

8.3. Spatial Distribution of Postseismic Deformation

[87] Although details of the afterslip distribution are poorly known due to a lack of data in critical locations, some features of the spatial distribution are robust. First, the largest peaks in the afterslip must have occurred downdip of the two main coseismic asperities in order to match the observed postseismic uplift. If there had been as much afterslip in the region between the asperities, the cumulative postseismic uplift would have been more uniform across the Kenai Peninsula, instead of being much larger in the eastern part than in the west. Similarly, in the Kodiak Island region the afterslip had to be larger in the eastern part compared to the west in order to explain the difference between postseismic uplift in the two parts of the island [*Sauber et al.*, 2006]. The first-order spatial distribution of afterslip is consistent with larger afterslip occurring where the coseismic stress changes were larger which would result if the magnitude of afterslip was proportional to the coseismic shear stress (or Coulomb stress) change.

[88] The recent M_w = 8.0 2003 Tokachi-Oki earthquake, northeast Japan, was followed by afterslip that extended not just downdip of the coseismic rupture, but also along strike from there [*Miyazaki et al.*, 2004; *Ozawa et al.*, 2004]. There is some evidence for the 1964 Alaska earthquake afterslip being more uniform along strike than the coseismic slip. In particular, the afterslip peak for Kodiak Island is broader along strike than the coseismic slip peak, and in our model there are places where the afterslip is roughly equal to the coseismic slip updip of it. However, there is no clear evidence for significant afterslip extending along strike beyond the ends of the 1964 earthquake rupture.

[89] The model and also the present GPS velocities show that the present postseismic deformation is largely confined within the along-strike limits of the coseismic rupture. This agrees with the estimate of *Zweck et al.* [2002a], using an afterslip-based model. Thus, even though the effects of viscoelastic relaxation extend at least one rupture length inland from the trench (~800 km), there is no evidence for significant postseismic effects beyond the ends of the rupture. *Hu et al.* [2004] found the same result for the 1960 Chile earthquake from GPS observations and modeling. Beyond the ends of the rupture they predicted a small component of trench-parallel postseismic deformation, but no trenchward motion.

8.4. Temporal Deformation History

[90] Several past studies have suggested that a combination of two characteristic relaxation time scales were present in the postseismic data [*Savage and Plafker*, 1991; *Zweck et al.*, 2002b; *Cohen and Freymueller*, 2004]. The earliest postseismic study, *Brown et al.* [1977], suggested a relaxation time of 2–3 years to explain the decay of uplift along Turnagain Arm of Cook Inlet. We found a similar result. The best fit afterslip history at tide gauge stations involves an exponential relaxation with a Maxwell time of 10 years, and additional deformation comes from the viscoelastic relaxation with a Maxwell time of 15–25 years. Similar viscosities to our best fitting range (2.3 to 3.9 $\times$ 10^{19} Pa s) are quite common in subduction zone based on postseismic deformation modeling [*Wang*, 2007]. These values are much lower than values based on global postglacial rebound analyses.

[91] An additional, much shorter, relaxation is also present in the data. The tide gauge at Kodiak shows extremely rapid uplift over the first few years, which we could not fit with any of the temporal decay functions we tested. This short relaxation process is similar to the rapid decay of early postseismic deformation observed by the leveling data at Turnagain Arm [*Brown et al.*, 1977]. It is extremely unfortunate that there was a ~20 year gap in data from the Kenai and Cook Inlet region starting in the mid-1970s; if we had more continuous data we might be able to distinguish the changing time scales and thus deformation mechanisms. We have to consider the possibility that afterslip following this earthquake decayed over two distinct time scales, which might represent a transition from frictional (rate and state) creep to a more ductile or viscous style of creep. This deformation must involve motion across a narrow shear zone, because a slip-like model can explain

it, but not a viscous flow model. The model of *Perfettini et al.* [2005] includes such a combination of failure mechanisms for the subduction interface downdip of the shallow seismogenic zone.

[92] One important feature in our model is that we include the viscoelastic relaxation caused by the afterslip, as well as that caused by the coseismic slip. Stress changes due to afterslip are, in general, much smaller than the coseismic stress changes, but the impact of afterslip is significant, and should be included in models of future earthquakes where the data distribution and precision will be (we hope) far superior to that of the 1964 Alaska earthquake. Afterslip tends to relax stress near the downdip end of the rupture faster than viscoelastic relaxation can, due to the difference in time scales involved, but it transfers stress downdip to the mantle wedge and thus enhances viscous flow in the wedge. The postseismic deformation model for Cascadia by *Wang et al.* [2001] simulated this by using a narrow low-viscosity shear zone downdip of the coseismic rupture.

9. Conclusions

[93] We constructed a 3-D viscoelastic model in concert with afterslip and an interseismic slip deficit model to examine the postseismic deformation following the 1964 Alaska earthquake. Our model incorporated a realistic geometry including an elastic slab with very low dip angle. These geometric factors were important, and this required a reanalysis of the 1964 coseismic slip model in order to make the most precise predictions of postseismic deformation.

[94] Our coseismic slip model is not based on an inversion, but our final model resembled the recently published inversion model and past models. The main difference in our model is that we propose that the high-angle splay fault on the Patton Bay fault extends as far as the western end of the Kenai Peninsula. Detailed submarine mapping may be required to test our hypothesis, although near-field tsunami arrival times may provide a test, because the tsunami will arrive earlier in our model with the splay fault and may have a different polarity. Given the model geometry and the coseismic slip model, we computed the deformation using a range of mantle viscosities ($\eta = 1.6 \times 10^{18}$ to 7.9×10^{19} Pa s), equivalent to Maxwell relaxation time τ of 1 to 50 years, and we selected a best model with $\tau = 20$ years ($\eta = 3.2 \times 10^{19}$ Pa s) based on the fit to the far-field present velocities, while including an interseismic elastic deformation model.

[95] Our modeling showed that no single mechanism could explain both the 30 year cumulative uplift and the present velocities, but a combination of viscoelastic relaxation, afterslip and interseismic slip deficit explain all first-order features of observed postseismic deformations. *Sauber et al.* [2006] found this same conclusion for Kodiak Island, and we can extend it to the entire rupture zone. Our model suggests that viscoelastic relaxation contributes to the total 30 to 35 years postseismic uplift moderately in the Kodiak region (40%), slightly in the western Kenai Peninsula (<20%) and not significantly in the northern Kenai Peninsula (<10%). The viscoelastic model has little impact on cumulative uplifts at Kodiak Island and the Kenai Peninsula, allowing us to use these data to constrain the afterslip distribution and time history. After removing the viscoelastic response, the largest residual cumulative uplifts were located downdip areas of largest coseismic slip area, requiring afterslip concentrated in those areas. Afterslip amounted to 3–4 m in the Kenai and Cook Inlet area and 3 m in the Kodiak Island area, with time history using exponential decay with $T = 10$ years. In addition to this, a large and rapidly decaying phase of early afterslip probably occurred, based on the tide gauge record from Kodiak and the repeated leveling at Turnagain Arm.

[96] Even 40 years after the earthquake, the present-day velocities contain a significant component of postseismic deformation, showing that very long lived postseismic deformation plays an important role in the subduction zone earthquake cycle for huge earthquakes. Our estimated afterslip temporal history suggests that the present rate of afterslip remains ~1 cm/yr, based mainly on the uplift record of the Kodiak tide gauge. Viscoelastic effects dominate the contribution of postseismic deformation to the present horizontal surface velocities, especially in the far field.

[97] We estimated interseismic elastic deformation models for every candidate postseismic model, and used the misfit of the overall model to the data north of 62°N and consistency with temporal history of afterslip to select the best viscoelastic relaxation time. The best fitting model, with a relaxation time of 20 years, provides the best fit to these far field data, and is requires a present rate of afterslip consistent with the total postearthquake temporal afterslip history. Models with relaxation times shorter than 15 years can be ruled out because they produce a poor fit to the data, and models with relaxation times longer than 25 years can be ruled out because they require rapid present afterslip that is inconsistent with the afterslip history.

[98] The residuals to the interseismic model are dominated by spatially coherent patterns that depend only weakly on the postseismic model used. These probably result from large-scale block motions of the overriding plate relative to North America. This interpretation prompts us to propose that a block of crust south of the active strike-slip Castle Mountain–Lake Clark–Bruin Bay faults and extending as far southeast as the Alaska Peninsula moves in a southeast, trench parallel, direction at a rate of ~5 mm/yr. Further work is required to refine this hypothesis and explore its ramifications.

[99] **Acknowledgments.** We are grateful to Steven C. Cohen for his helpful discussions on postseismic uplift in the Kenai Peninsula and numerical technique of FEM and to Jeanne Sauber and Kelin Wang for helpful reviews and editing. Part of this research was supported by Research Fellowships of the JSPS for Young Scientists to H.S. J.F. was supported by the U.S. National Science Foundation grant EAR-0409950, and GPS field observations used here were supported by NSF grants EAR-9706318, EAR-9805326, EAR-9980496, EAR-9973189, EAR-0106829, and EAR-0207957 and by the USGS NEHRP program. Figures 1–13 were created with the Generic Mapping Tools (GMT) software [*Wessel and Smith*, 1998].

References

Brocher, T. M., G. S. Fuis, M. A. Fisher, G. Plafker, M. J. Moses, J. J. Taber, and N. I. Christensen (1994), Mapping the megathrust beneath the northern Gulf of Alaska using wide-angle seismic data, *J. Geophys. Res.*, *99*, 11,663–11,685, doi:10.1029/94JB00111.

Brown, L. D., R. E. Reilinger, S. R. Holdahl, and E. I. Balazs (1977), Postseismic crustal uplift near Anchorage, Alaska, *J. Geophys. Res.*, *82*, 3369–3378, doi:10.1029/JB082i023p03369.

Christensen, D. H., and S. L. Beck (1994), The rupture process and tectonic implications of the great 1964 Prince William Sound earthquake, *Pure Appl. Geophys.*, *142*, 29–53, doi:10.1007/BF00875967.

Cohen, S. C. (1996), Time-dependent uplift of the Kenai Peninsula and adjacent regions of south central Alaska since the 1964 Prince William Sound earthquake, *J. Geophys. Res.*, *101*, 8595–8604, doi:10.1029/96JB00175.

Cohen, S. C., and J. T. Freymueller (1997), Deformation of the Kenai Peninsula, Alaska, *J. Geophys. Res.*, *102*, 20,479–20,487, doi:10.1029/97JB01513.

Cohen, S. C., and J. T. Freymueller (2004), Crustal deformation in the southcentral Alaska subduction zone, *Adv. Geophys.*, *47*, 1–58.

Cohen, S. C., S. Holdahl, D. Caprette, S. Hilla, R. Safford, and D. Schultz (1995), Uplift of the Kenai Peninsula, Alaska, since the 1964 Prince William Sound earthquake, *J. Geophys. Res.*, *100*, 2031–2038, doi:10.1029/94JB02880.

Cross, R., and J. T. Freymueller (2007), Plate coupling variation and block translation in the Andreanof segment of the Aleutian Arc determined by subduction zone modeling using GPS data, *Geophys. Res. Lett.*, *34*, L06304, doi:10.1029/2006GL028970.

Doser, D. I., A. M. Veilleux, and M. Velasquez (1999), Seismicity of the Prince William Sound Region for over thirty years following the 1964 great Alaskan earthquake, *Pure Appl. Geophys.*, *154*, 593–632, doi:10.1007/s000240050246.

Fletcher, H. J. (2002), Crustal deformation in Alaska measured using the Global Positioning System, Ph.D. thesis, 135 pp., Univ. of Alaska Fairbanks, Fairbanks.

Fletcher, H. J., and J. T. Freymueller (2003), New constraints on the motion of the Fairweather fault, Alaska, from GPS observations, *Geophys. Res. Lett.*, *30*(3), 1139, doi:10.1029/2002GL016476.

Fournier, T. J., and J. T. Freymueller (2007), Transition from locked to creeping subduction in the Shumagin region, Alaska, *Geophys. Res. Lett.*, *34*, L06303, doi:10.1029/2006GL029073.

Freymueller, J. T. (2005), Real time GPS magnitudes for the largest earthquakes, and application to tsunami warning, *Eos Trans. AGU*, *86*(18), Jt. Assem. Suppl., Abstract U51A-05.

Freymueller, J. T., S. C. Cohen, and H. J. Fletcher (2000), Spatial variations in present-day deformation, Kenai Peninsula, Alaska, and their implications, *J. Geophys. Res.*, *105*, 8079–8101, doi:10.1029/1999JB900388.

Freymueller, J. T., H. Woodard, S. C. Cohen, R. Cross, J. Elliott, C. F. Larsen, S. Hreinsdottir, and C. Zweck (2008), Active deformation processes in Alaska, based on 15 years of GPS measurements, in *Active Tectonics and Seismic Potential of Alaska*, *Geophys. Monogr. Ser.*, vol. 179, edited by J. T. Freymueller, P. J. Haeussler, R. L. Wesson, and G. Ekstrom, 1–42, doi:10.1029/179GM02, AGU, Washington, D. C.

Furumoto, A. S. (1965), Analysis of Rayleigh wave, part II, in *Source Mechanism Study of the Alaska Earthquake and Tsunami of March 27, 1964*, *Rep. HIG-65–17*, pp. 31–42, Inst. Of Geophys., Univ. of Hawaii, Honolulu.

Gilpin, L. M. (1995), Holocene paleoseismicity and coastal tectonics of the Kodiak Islands, Alaska, Ph.D. thesis, 357 pp., Univ. of Calif., Santa Cruz.

Gilpin, L. M., G. A. Carver, S. Ward, and R. S. Anderson (1994), Tidal benchmark readings and postseismic rebound of the Kodiak Islands, SW extent of the 1964 great Alaskan earthquake rupture zone, *Seismol. Res. Lett.*, *65*(1), 68.

Gregorius, T. (1996), *GIPSY-OASIS II: A User's Guide*, Univ. of Newcastle, Newcastle, U. K.

Harris, R. A., and P. Segall (1987), Detection of locked zone at depth on the Parkfield, California segment of the San Andreas fault, *J. Geophys. Res.*, *92*, 7945–7962, doi:10.1029/JB092iB08p07945.

Holdahl, S. R., and J. Sauber (1994), Coseismic slip in the 1964 Prince William Sound earthquake: A new geodetic inversion, *Pure Appl. Geophys.*, *142*, 55–82, doi:10.1007/BF00875968.

Hu, Y., K. Wang, J. He, J. Klotz, and G. Khazaradze (2004), Three-dimensional viscoelastic finite element model for postseismic deformation of the great 1960 Chile earthquake, *J. Geophys. Res.*, *109*, B12403, doi:10.1029/2004JB003163.

Ichinose, G., P. Somerville, H. K. Thio, R. Graves, and D. O'Connell (2007), Rupture process of the 1964 Prince William Sound, Alaska, earthquake from the combined inversion of seismic, tsunami, and geodetic data, *J. Geophys. Res.*, *112*, B07306, doi:10.1029/2006JB004728.

Iizuka, M., D. Sekita, H. Suito, M. Hyodo, K. Hirahara, D. Place, P. Mora, O. Hazama, and H. Okuda (2002), Parallel simulation system for earthquake generation: Fault analysis modules and parallel coupling analysis, *Concurr. Comput.*, *14*, 499–519, doi:10.1002/cpe.628.

Johnson, J. M., K. Satake, S. R. Holdahl, and J. Sauber (1996), The 1964 Prince William Sound earthquake: Joint inversion of tsunami and geodetic data, *J. Geophys. Res.*, *101*, 523–532, doi:10.1029/95JB02806.

Kanamori, H. (1970), The Alaska earthquake of 1964: Radiation of long-period surface waves and source mechanism, *J. Geophys. Res.*, *75*, 5029–5040, doi:10.1029/JB075i026p05029.

Lahr, J. C., and G. Plafker (1980), Holocene Pacific-North American plate interaction in southern Alaska: Implications for the Yakataga seismic gap, *Geology*, *8*, 483–486, doi:10.1130/0091-7613(1980)8<483:HPAPII>2.0.CO;2.

Larsen, C. F., K. A. Echelmeyer, J. T. Freymueller, and R. J. Motyka (2003), Tide gauge records of uplift along the northern Pacific-North American plate boundary, 1937 to 2001, *J. Geophys. Res.*, *108*(B4), 2216, doi:10.1029/2001JB001685.

Larsen, C. F., R. J. Motyka, J. T. Freymueller, K. A. Echelmeyer, and E. R. Ivins (2005), Rapid viscoelastic uplift in southeast Alaska caused by post-Little Ice Age glacial retreat, *Earth Planet. Sci. Lett.*, *237*, 548–560, doi:10.1016/j.epsl.2005.06.032.

Marone, C. J., C. H. Scholz, and R. Bilham (1991), On the mechanics of earthquake afterslip, *J. Geophys. Res.*, *96*, 8441–8452, doi:10.1029/91JB00275.

Masterlark, T. (2003), Finite element model predictions of static deformation from dislocation sources in a subduction zone: Sensitivities to homogeneous, isotropic, Poisson-solid, and half-space assumptions, *J. Geophys. Res.*, *108*(B11), 2540, doi:10.1029/2002JB002296.

Melosh, H. J., and A. Raefsky (1981), A simple and efficient method for introducing faults into finite element computations, *Bull. Seismol. Soc. Am.*, *71*, 1391–1400.

Miyazaki, S., P. Segall, J. Fukuda, and T. Kato (2004), Space time distribution of afterslip following the 2003 Tokachi-oki earthquake: Implications for variations in fault zone frictional properties, *Geophys. Res. Lett.*, *31*, L06623, doi:10.1029/2003GL019410.

Moore, J. C., J. Diebold, M. A. Fisher, J. Sample, T. Brocher, M. T. J. Ewing, R. von Huene, C. R. D. Stone, C. Stevens, and D. Sawyer (1991), EDGE deep seismic reflection transect of the eastern Aleutian arc-trench layered lower crust reveals underplating and continental growth, *Geology*, *19*, 420–424, doi:10.1130/0091-7613(1991)019<0420:EDSRTO>2.3.CO;2.

Nettles, M., G. Ekstrom, A. M. Dziewonski, and N. Maternovskaya (2005), Source characteristics of the great Sumatra earthquake and its aftershocks, *Eos Trans. AGU*, *86*(18), Jt. Assem. Suppl., Abstract U43A-01.

Ohta, Y., J. T. Freymueller, S. Hreinsdottir, and H. Suito (2006), A large slow slip event and the depth of the seismogenic zone in the south central Alaska subduction zone, *Earth Planet. Sci. Lett.*, *247*, 108–116, doi:10.1016/j.epsl.2006.05.013.

Okuda, H., and G. Yagawa (2001), Large-scale parallel finite element analysis for solid earth problems by GeoFEM, *RIST/TOKYO GeoFEM Rep. 2001-001*, Res. Organ. for Inf. Sci. and Technol., Tokyo. (Available at http://geofem.tokyo.rist.or.jp/report_en/2001_001.html)

Oleskevich, D. A., R. D. Hyndman, and K. Wang (1999), The updip and downdip limits to great subduction earthquake: Thermal and structural models of Cascadia, south Alaska, SW Japan, and Chile, *J. Geophys. Res.*, *104*, 14,965–14,991, doi:10.1029/1999JB900060.

Ozawa, S., M. Kaidzu, M. Murakami, T. Imakiire, and Y. Hatanaka (2004), Coseismic and postseismic crustal deformation after the Mw8 Tokachi-oki earthquake in Japan, *Earth Planets Space*, *56*, 675–680.

Page, R. A., N. N. Biswas, J. C. Lahr, and H. Pulpan (1991), Seismicity of continental Alaska, in *Neotectonics of North America, Decade Map*, vol. 1, edited by D. B. Slemmons et al., pp. 47–68, Geol. Soc. of Am., Boulder, Colo.

Parkin, E. J. (1972), Horizontal crustal movements, in *The Great Alaska Earthquake of 1964, Seismology and Geodesy*, pp. 419–434, Natl. Acad. of Sci., Washington, D. C.

Paul, J., A. R. Lowry, R. Bilham, S. Sen, and R. Smalley Jr. (2007), Postseismic deformation of the Andaman Islands following the 26 December, 2004 Great Sumatra-Andaman earthquake, *Geophys. Res. Lett.*, *34*, L19309, doi:10.1029/2007GL031024.

Perfettini, H., J.-P. Avouac, and J.-C. Ruegg (2005), Geodetic displacements and aftershocks following the 2001 Mw = 8.4 Peru earthquake: Implications for the mechanics of the earthquake cycle along subduction zones, *J. Geophys. Res.*, *110*, B09404, doi:10.1029/2004JB003522.

Piersanti, A., G. Spada, and R. Sabadini (1997), Global postseismic rebound of a viscoelastic Earth: Theory for finite faults and application to the 1964 Alaska earthquake, *J. Geophys. Res.*, *102*, 477–492, doi:10.1029/96JB01909.

Plafker, G. (1972), Tectonics, in *The Great Alaska Earthquake of 1964, Seismology and Geodesy*, pp. 113–188, Natl. Acad. of Sci., Washington, D. C.

Pollitz, F., P. Banerjee, K. Grijalva, B. Nagarajan, and R. Burgmann (2008), Effect of 3-D viscoelastic structure on post-seismic relaxation from the 2004 *M* = 9.2 Sumatra earthquake, *Geophys. J. Int.*, *173*, 189–204, doi:10.1111/j.1365-246X.2007.03666.x.

Santini, S., M. Dragoni, and G. Spada (2003), Asperity distribution of the 1964 great Alaska earthquake and its relation to subsequent seismicity in the region, *Tectonophysics*, *367*, 219–233, doi:10.1016/S0040-1951(03)00130-6.

Sauber, J., G. Carver, S. Cohen, and R. King (2006), Crustal deformation and the seismic cycle across the Kodiak Islands, Alaska, *J. Geophys. Res.*, *111*, B02403, doi:10.1029/2005JB003626.

Savage, J. C., and G. Plafker (1991), Tide gage measurements of uplift along the south coast of Alaska, *J. Geophys. Res.*, *96*, 4325–4335, doi:10.1029/90JB02540.

Savage, J. C., J. L. Svarc, W. H. Prescott, and W. K. Gross (1998), Deformation across the rupture zone of the 1964 Alaska earthquake, 1993–1997, *J. Geophys. Res.*, *103*, 21,275–21,283, doi:10.1029/98JB02048.

Savage, J. C., J. L. Svarc, and W. H. Prescott (1999), Deformation across the Alaska-Aleutian subduction zone near Kodiak, *Geophys. Res. Lett.*, *26*, 2117–2120, doi:10.1029/1999GL900471.

Small, J. B., and L. C. Wharton (1972), Vertical displacements, in *The Great Alaska Earthquake of 1964, Seismology and Geodesy*, pp. 449–461, Natl. Acad. of Sci., Washington, D. C.

Snay, R. A., M. W. Cline, and E. L. Timmerman (1987), Project REDEAM: Models for historical horizontal deformation, *Tech. Rep. NOS 125 NGS 42*, Natl. Geod. Surv., NOAA, Silver Spring, Md.

Stout, J. H., and C. G. Chase (1980), Plate kinematics of the Denali fault system, *Can. J. Earth Sci.*, *17*(11), 1527–1537.

von Huene, R., D. Klaeschen, and J. Fruehn (1999), Relation between the subducting plate and seismicity associated with the great 1964 Alaska earthquake, *Pure Appl. Geophys.*, *154*, 575–591, doi:10.1007/s000240050245.

Wang, K. (2007), Elastic and viscoelastic models of subduction earthquake cycles, in *The Seismogenic Zone of Subduction Thrust Faults*, edited by T. H. Dixon and J. C. Moore, pp. 540–575, Columbia Univ. Press, New York.

Wang, K., J. He, H. Dragert, and T. S. James (2001), Three-dimensional viscoelastic interseismic deformation model for the Cascadia subduction zone, *Earth Planets Space*, *53*, 295–306.

Ward, S., and S. E. Barrientos (1986), An inversion for slip distribution and fault shape from geodetic observations of the 1983, Borah Peak, Idaho, earthquake, *J. Geophys. Res.*, *91*, 4909–4919, doi:10.1029/JB091iB05p04909.

Wessel, P., and W. H. F. Smith (1998), New improved version of the Generic Mapping Tools released, *Eos Trans. AGU*, *79*, 579, doi:10.1029/98EO00426.

Wolf, L. W., D. B. Stone, and J. N. Davies (1991), Crustal structure of the active margin, south central Alaska: An interpretation of seismic refraction data from the Trans-Alaska Crustal Transect, *J. Geophys. Res.*, *96*, 16,455–16,469, doi:10.1029/91JB01482.

Yoshioka, S., and H. Suzuki (1999), Effects of three-dimensional inhomogeneous viscoelastic structures on postseismic surface deformations associated with the great 1946 Nankaido earthquake, *Pure Appl. Geophys.*, *154*, 307–328, doi:10.1007/s000240050231.

Zumberge, J. F., M. B. Heflin, D. C. Jefferson, M. M. Watkins, and F. H. Webb (1997), Precise point positioning for the efficient and robust analysis of GPS data from large networks, *J. Geophys. Res.*, *102*, 5005–5017, doi:10.1029/96JB03860.

Zweck, C., J. T. Freymueller, and S. C. Cohen (2002a), Three-dimensional elastic dislocation modeling of the postseismic response to the 1964 Alaska earthquake, *J. Geophys. Res.*, *107*(B4), 2064, doi:10.1029/2001JB000409.

Zweck, C., J. T. Freymueller, and S. C. Cohen (2002b), The 1964 great Alaska earthquake: Present day and cumulative postseismic deformation in the western Kenai Peninsula, *Phys. Earth Planet. Inter.*, *132*, 5–20, doi:10.1016/S0031-9201(02)00041-9.

J. T. Freymueller, Geophysical Institute, University of Alaska Fairbanks, Fairbanks, AK 99775, USA.

H. Suito, Geography and Crustal Dynamics Research Center, Geographical Survey Institute, Tsukuba 305-0811, Japan. (suito@gsi.go.jp)